Results in Engineering 24 (2024) 103454

Contents lists available at ScienceDirect

Results in Engineering

journal homepage: www.sciencedirect.com/journal/results-in-engineering

Research paper

Advanced predictive modeling of shear strength in stainless-steel column web panels using explainable AI insights

Sina Sarfarazi [a], Rabee Shamass [b,*], Federico Guarracino [a], Ida Mascolo [a], Mariano Modano [a]

[a] Department of Structures for Engineering and Architecture, University of Naples "Federico II", Naples, 80125, Italy
[b] Department of Civil and Environmental Engineering, Brunel University London, London, UK

ARTICLE INFO

Keywords:
Moment-resisting steel frames
Shear strength of panel zones
Stainless-steel structures
Data-driven models
Interpretable machine learning

ABSTRACT

In steel moment-resisting frames, energy dissipation occurs through yielding at the beam ends. Furthermore, the column panel zone can be designed to contribute to this energy dissipation process. The European standard (EN 1993–1–4) for stainless-steel is developed based on carbon steel procedures, without taking into account stainless steel's unique strain hardening and mechanical properties. This discrepancy may result in inaccuracies in predicting panel zone behavior. However, with the recent advancements in stainless steel, it is timely to reassess these limitations. The present research investigates the behavior of stainless-steel column web panels through an explainable artifactual intelligence methodology. This approach combines twelve widely recognized machine learning algorithms with the SHAP algorithm for enhanced explainability and transparency. In addition, a user-friendly graphical user interface has been developed to simplify engineering design. The Extra Trees Regression algorithm demonstrated the highest predictive performance, achieving $R^2 = 0.987$, mean absolute error (MAE) = 3.575 kN, and root mean square error (RMSE) = 6.464 kN for the entire dataset. The SHAP analysis revealed that bolt diameter and the column second moment of inertia are the most critical input features affecting shear strength. This approach effectively captures the nonlinear characteristics of shear behavior in stainless-steel column web panels and offers clear insights into the contribution of different factors. The developed method not only improves predictive accuracy but also promotes transparency, making it a practical tool for engineers in structural component design.

1. Introduction

The use of stainless-steel as a structural material has greatly advanced due to the recent trend in the use of sustainable materials with improved performance [1]. This material's exceptional corrosion resistance and durability make it the ideal choice for use in harsh environments, such as coastal or industrial areas [1,2]. Furthermore, stainless steel's recyclability and long lifespan align with current trends toward sustainable construction practices, where reducing environmental impact is key. In this regard, recent studies have also explored eco-friendly materials, such as recycled concrete and brick waste, to further reduce the carbon footprint of construction materials [3–6]. Long-lasting structures minimize the expenses of regular maintenance and as well increase their lifespan, which is in line with increased acceptance of sustainable building [7]. Furthermore, stainless-steel is an optimal material in terms of strength-to-weight, making it possible to build light and slender constructions without compromising structural stability or safety. This attribute can mean significant financial and engineering advantages [8]. It also meets the current architectural requirement of designing attractive architectural structures since this material allows for development of slender and aesthetically pleasing components [9]. Stainless-steel exhibits non-linear behavior at relatively low-stress levels, unlike carbon-steel. However, it does not show a defined yield stress or a distinct plateau before undergoing strain hardening. Rather, as strain rises, the stress-strain diagrams show a progressive reduction in stiffness and notable strain hardening [10]. Moreover, greater elongation ability of stainless-steel in the plastic zone, between the yield strength and ultimate tensile strength, can be attributed to its high ductility characteristic [2,8]. In cold working process that is used for stainless-steel, work hardening is improved which further leads to increased strengths and hardness. The unique properties of stainless-steel make it an optimal material for improving the seismic resilience of building structures [11]. In practice, the majority of international structural design standards, for example the current EN

* Corresponding author.
E-mail address: Rabee.Shamass@brunel.ac.uk (R. Shamass).

https://doi.org/10.1016/j.rineng.2024.103454
Received 14 October 2024; Received in revised form 11 November 2024; Accepted 18 November 2024
Available online 19 November 2024

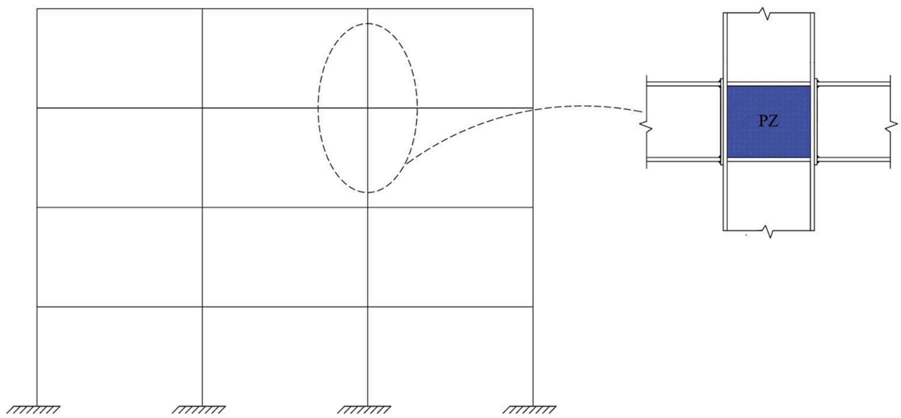

Fig. 1. Panel zone in steel frame.

1993–1–8 design [12], refer to the design of carbon-steel structures. They only offer supplementary guidelines for the design of stainless-steel structures (Eurocode 3 (EN 1993–1–4) [13] design codes). This raises concerns regarding the utilization of these steels in numerous structural applications.

A moment-resisting frame (MRF) is capable of resisting lateral force by inducing flexural and shear behavior in the beams and columns and is thus a good choice for lateral load-resistance systems [14]. MRF can be considered very important in architectural as well as functional adaptability. In addition, beam-column connections are critical in the structural integrity of MRFs because they are the primary components that resist the seismic forces. The degree of moment transmission among its constituent parts is the key to the performance of an MRF. During both the Northridge and Kobe earthquakes, numerous structures experienced weld fractures, leading to significant failures. As a result, researchers began exploring high-strength bolted connections that show semi-rigid characteristics [15], such as Flush end-plate connections (FECs). These bolted connections in frame systems have proven effective in minimizing various types of damage during earthquake loads. FECs are generally considered a viable alternative to beam-to-column joints in moment-resisting frames [15]. FECs are made of a connecting plate that is welded to the beam flange and bolted to the column through the use of high tensile bolts. Nevertheless, the structural performance can be influenced by inaccurate interpretations of FECs behavior. It is therefore important to design FECs according to their actual structural behavior. As for the plastic design, FECs also offer sufficient rotation capacity. Furthermore, it is crucial to note that the interaction forces between the components can affect the behavior of the connection. In nonlinear analysis, beam-column joints may yield in shear since they have to transfer considerable bending moment [16]. Not considering the fact that joints are relatively flexible compared to other structural components, this can cause incorrect hinge formation patterns. As a result, it is necessary to have a separate component that properly simulates the behavior of the beam-column joint. To overcome this, a panel zone (PZ) joint component is introduced for the purpose of idealizing steel beam-column joints for nonlinear analysis of MRFs [17]. The panel zone, as depicted in Fig. 1, is the column region enclosed by continuity plates and column flanges. The integration of the panel zone into the moment-resisting frames design has both advantages and disadvantages. On the positive side, the panel zone can play a major role in energy dissipation through inelastic deformation and thus increasing the overall ductility of the frame and the distribution of seismic energy.

This also means that less damage is caused to crucial elements like beams and helps to enhance the strength of the structure during earthquake. Also, when the panel zone is designed to contribute to energy absorption it allows for the optimization of the balance between strength and ductility according to specific performance objectives. However, these benefits involve certain compromises. Permitting inelastic deformation in the panel zone can also cause large story displacements which affect the serviceability of the structure and hence additional drift control measures will be necessary. The reduction in overall structural stiffness due to inelastic panel zone behavior may affect lateral stability and necessitate additional design measures. In addition, higher strain demands increase the risk for local failure mechanisms. The performance of the panel zone has been of interest to researchers for decades. Investigations in this line started in late 1960s and early 1970s, and regulations and guidelines during this period addressed different aspects of panel zone response. In the conducted studies, emphasis has been put on the assessment performance of the panel zone in I-shaped open columns made of carbon steel. Krawinkler et al. [18] have pointed out the fact that panel zones demonstrate a high degree of strength after achieving the yield point. In these studies, the hysteretic loops that were deformable and stable and a high cyclic re-hardening was observed by the researchers. In addition, some studies have shown that shear deformations have a great influence on panel zone response [19]. The panel zone can adequately dissipate energy through shear up to a level that is characterized by considerable inelastic distortions and thus prevent local crippling and yielding of the column web and distortion of the column flange [16]. In terms of the panel zone, the process of shear yielding starts in the middle and then extends radially outward [19]. It can be observed that the shear distortion is at its maximum in the center of the panel zone and at minimum in the corner. In most cases when the connection is subjected to unbalanced bending moments, a panel zone experiences a complex pattern of stress [16]. This includes the normal stresses which mainly result from the axial force acting on the column, and the shear stress which occurs due to the moment which is transferred from the beams [20]. Studies on the behavior of panel zones in the elastic range have revealed the influence of shear distortion as highlighted by Krawinkler et al. [18]. Upon yielding, the shear strength of the panel zone, which is formed by the column flanges and continuity plates is greatly reduced. Based on Krawinkler et al. [18] findings, it is possible to state that the complete yield of the steel panel zones takes place at the distortion level that is four times higher than the initial one. This assumption is also considered in the current design standards.

Most of the studies on the panel zones have been performed on carbon and high strength steel columns. Jaspart [21] used numerical and experimental analysis to study the behavior of the panel zone and to propose multi-linear analytical models. These models were introduced in EN 1993–1–8 [12] later. Coelho et al. [22] undertook a series of experiments on web shear panels of high strength steel to assess the shear strength performance and the results compared with that of the design codes currently in use. Jordao et al. [23] using experimental and numerical investigations proposed a new mechanical model to analyze internal carbon steel joints with beams of unequal depths. Tuna et al. [24] performed a numerical analysis to determine the deformation requirements in carbon steel panel zones which were designed in accordance with various code provisions. They conducted a parametric study, and the analyses revealed that designs based on EN 1993–1–8 [12] resulted in negligible yielding in the panel zone. Brandonisio et al. [25] assessed the mechanical characteristics of the beam to column panel zone and reviewed the European code for the design of PZs. The analysis includes non-linear numerical and experimental tests. The results are then compared with the practices followed in Europe. The study, both theoretical and experimental, has identified some shortcomings in the application of the European regulations, leading to an over estimation of PZ shear strength by approximately 50–60 %. Lu et al. [26] compared the mechanical properties of the panel zone through testing end-plate and T-stub connections under cyclic loading. They compared the parameters like shear force, plastic energy dissipation, and failure modes. Comparing the available experimental and analytical data, it is possible to point out that even in cases with carbon steel I-sections having flange thicknesses greater than 2.5 cm, the provided models in the design codes are not adequately precise [16]. This underlines the need for a design criterion that is safer and more dependable, especially in the case of stainless steel. Unlike carbon steel, stainless-steel exhibits significantly different mechanical behaviors.

Conducting experiments to assess the shear strength of stainless-steel column web panels is expensive. The development of steel design through analytical, empirical, mechanical, and numerical simulation models has been greatly enhanced yet the design process still remains a laborious task and offers limited support for design enhancement. Analytical method constitutes a mathematically accurate and computationally efficient prediction technique through the use of mathematical equations, but its effectiveness is, however, limited in significant deformations or high static complexity. The empirical curve fitting method, though being straightforward and practical for engineers who do not have many computation resources, suffers from the accuracy and reliability, especially in complex steel joints. The component method offers a detailed description of connection behavior by modeling discrete elements like bolts and plates, though its complexity demands extensive component data. Finite element modelling is a notable technique as it allows to simulate complex features and behaviors, nonlinearities and material specifics, with insights into stress, strain and failure mechanisms. However, its computational demands and the expertise required for effective use pose significant challenges, particularly for those with constrained resources. More recently, there has been a shift towards computational methods where computers learn from data samples, known as the machine learning (ML) approach. ML is gaining more importance in the field of structural engineering as it integrates artificial intelligence (AI) with the intricacies of engineering design and safety [27]. This study's ML approach, combined with explainable artificial intelligence (XAI) techniques, provides a novel alternative. By employing ML models, this approach captures nonlinear behaviors and interactions in the shear behavior of stainless-steel column web panels with high accuracy and efficiency. Integration of the SHapley Additive exPlanations (SHAP) algorithm further ensures interpretability by revealing the influence of critical input features on shear strength predictions. This combination enhances both the reliability and transparency of the model's predictions, offering a practical and accessible tool for design engineers and researchers. ML techniques have been applied in different fields, for example, applying Support Vector Regression (SVR) for fatigue reliability of offshore wind structures for the treatment of uncertainties in material and load characteristics [28], and ML models for detection of seismic failure modes in concrete structures [29]. Due to the benefits of ML in predicting structural responses, some researchers have incorporated adaptative frameworks with Monte Carlo simulations to improve computation time in the reliability analysis of complex structures [30]. Shah et al. [31] explored the application of ML models to predict the moment-rotation behavior of boltless steel connections, employing Artificial Neural Networks (ANN), Adaptive Neuro-Fuzzy Inference System (ANFIS), and Linear Genetic Programming (LGP). The study demonstrated that, while ANN and ANFIS models showed limitations in accurately modeling nonlinear relationships, the LGP model outperformed both, providing superior predictive accuracy and robustness. Cao et al. [32] investigated the use of the Extreme Learning Machine (ELM) method to predict the moment behavior in beam-to-column connections. The study aimed to address the limitations of traditional approaches by applying ELM to model complex, nonlinear relationships with high accuracy and reduced computational time. The authors compared ELM's performance to Genetic Programming (GP) and ANN, finding that ELM outperformed both in terms of prediction accuracy. The results indicated that ELM could effectively capture the moment-rotation characteristics and provide reliable estimates. Kueh [33] developed mathematical expressions for the moment-rotation behavior of steel flush endplate beam-column connections using ANN and Multi-Linear Regression (MLR). The study addressed limitations of existing models by providing explicit equations for resistant moment and initial rotational stiffness. The ANN model, trained using MATLAB, showed superior predictive performance compared to MLR, with higher correlation coefficients and lower mean absolute percentage error (MAPE). This work highlights the potential of ANN to generate ready-to-use equations for structural design, reducing computational and experimental complexities.

So far, ML models have only been used to address the shear behavior of reinforced concrete (RC) structural joints. However, no previous research seems to have examined the use of ML algorithms to predict the shear strength of steel column web panels. In this regard, several research have investigated the application of ML methods in predicting the shear capacity of exterior and interior concrete beam-column joints [34–36]. Similarly, ANN methods were applied by Alwanas et al. [37], and Park et al. [38] to predict the shear resistance of such joints. ML approaches have also been applied to estimate the shear transfer strength of RC joints [39]. Recently, Zakir Sarothi et al. [40] evaluated the performance of various ML models, including ANN, K-Nearest Neighbors (KNN), Support vector machines (SVM), Decision Tree (DT), Random Forest (RF), Extreme Gradient Boosting (XGBoost), and Categorical Boosting (CatBoost), to predict the bearing capacity of shear bolted connections. Furthermore, references [41,42] provide a comprehensive comparative analysis of the performance of various ML algorithms. These investigations have demonstrated that the ML predictions are highly accurate in predicting structural response of beam to column joints. In combination, these papers underscore the increasing use of ML in structural analysis and support the case for its further use to predict the structural component behavior with a high degree of accuracy and reliability.

To the best of the author's knowledge, a research gap exists in the study of stainless-steel column web panels, in contrast to the well-documented investigations on concrete, carbon steel, and high-strength steel joints. In fact, there appears to be no research addressing the shear strength of column web panels made of stainless-steel material. The methodology of this study begins with the development of an extensive input database using ABAQUS software and its integrated Python scripting interface [43]. During the training phase, then twelve well-established ML models are evaluated: Kernel Ridge Regression (KRR), Polynomial regression (PR), Decision Tree (DT), Random Forest (RF), Extremely Randomized Trees (ETR), K-Nearest Neighbors (KNN), Gradient Boosting (GB), Extreme Gradient Boosting (XGB), Light Gradient Boosting (LGBM), Categorical Boosting (CatBoost), Histogram-Based Gradient Boosting (HistGB), and Support Vector Regressor (SVR). In addition, the best optimal predictive model is determined considering the level of accuracy that is being achieved for shear strength. The next stage of the study focuses on the explanation of ML results. XAI provides a clearer picture of the input-output interconnections in the developed ML models. To achieve this goal, the SHAP algorithm is used, which provides explanations for the predictions made by ML. The SHAP is theoretically well-founded and can be used with any ML model, including shallow architecture and deep learning models. Local and global interpretations can be provided through this

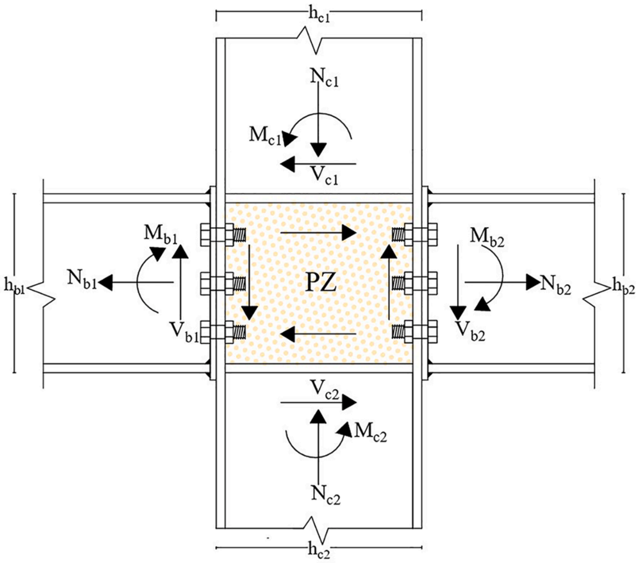

Fig. 2. Forces acting on PZ of an internal flush end-plate joint.

framework, which increases the understanding of the problem under consideration. Furthermore, the trained ML models are employed for designing a graphical user interface (GUI) software. By incorporating a GUI, it is possible for the researchers and designers to estimate the shear strength of stainless-steel column web panels, which increases the user-friendliness of the proposed method.

1.1. Contribution to the field and study significance

The objective of this study is to investigate the application of AI methods in predicting the shear behavior of column web panels using an XAI approach. This research will emphasize various important aspects:

- **Novelty**: This study is among the pioneering efforts to apply advanced ML techniques to predict the shear strength of H-shaped stainless-steel column web panels. It extends design considerations specifically to stainless-steel panel zones, a critical area currently limited by European standards, such as Eurocode 3 (EN 1993–1–4), which predominantly developed based on carbon steel.
- **Innovation and transparency:** This work uniquely integrates explainable AI techniques through the SHAP algorithm to interpret ML predictions. Unlike traditional black-box models, this approach gives a detailed description of why a certain model made a particular prediction, which has enhanced the interpretability of ML models. Such transparency can attract more research attention to the importance of interpretability and trustworthiness in predictive models.
- **Practicality:** The development of a simple GUI enhances the accessibility and usability of the predictive approach. This GUI could make it easy for researchers and designers to estimate the shear strength of stainless-steel column web panels, leading to broader applications of the method.

By addressing these aspects, this study fills a research gap in existing standards and research by providing a predictive framework developed specifically to the unique properties of stainless steel, which differ substantially from those of carbon steel. This work not only addresses the need for updated design considerations for stainless-steel, but also demonstrates the power of ML and XAI in advancing the field of structural engineering.

2. Panel zone shear strength

Fig. 2 shows the forces acting in the panel zone region. It is assumed that the joint members, beams, columns, and the panel zone has undergone bending moment (M), axial force (N), and shear force (V) due to horizontal earthquake load. The combined effect of these forces creates complex deformation and stress state of the panel zone region which makes the analysis of mechanical properties of the panel zone rather complex.

To obtain the shear force within the panel zone, the bending moment at the middle of the thickness of the beam flange may be used, given that the contraflexure point is located at mid-height of the columns. By considering the equilibrium relationship between the moment, axial and shear forces of the joint panel zone, the following relationship can be derived [25]:

$$\left(\frac{M_{b1}}{h_{b1}}+\frac{N_{b1}}{2}\right)+\left(\frac{M_{b2}}{h_{b2}}+\frac{N_{b2}}{2}\right)-V_{c1}-V_{pz}=0 \tag{1}$$

The global relationship between the force distribution of the panel zone is given by

$$N_{b1}-N_{b2}=V_{c1}-V_{c2} \tag{2}$$

And, by substituting Eq. (2) into Eq. (1), the shear force of the panel zone can be computed as

$$V_{pz}=\frac{M_{b1}}{h_{t1}}+\frac{M_{b2}}{h_{t2}}-\frac{V_{c1}+V_{c2}}{2}=\frac{M_{b1}}{h_{t1}}+\frac{M_{b2}}{h_{t2}}-V_c \tag{3}$$

In the above Eqs. (1–3), M_{b1} and M_{b2} represent the bending moments at the left and right ends of the beam, respectively. N_{b1} and N_{b2} denote the axial forces at the left and right beam ends. V_{c1} and V_{c2} are the shear forces in the column above and below the panel zone. h_{b1} and h_{b2} indicate the distances between the flanges of the left and right beams, while h_{c1} and h_{c2} represent the distances between the top and bottom column flanges.

The average shear strength value of the column section is determined by considering the equilibrium condition of the joint ($M_{c1}+M_{c2}=M_{b1}+M_{b2}$) [25]: (Eq. 4)

$$V_c=\frac{V_{c1}+V_{c2}}{2}=\frac{M_{c1}+M_{c2}}{H-d_b}=\frac{M_{b1}+M_{b2}}{H-d_b} \tag{4}$$

The shear strength value of the panel zone is determined by the following equation: (Eq. 5)

$$V_{pz}=\frac{M_{b1}+M_{b2}}{h_t}.(1-\beta) \tag{5}$$

where $h_t=(h_{b1}+h_{b2})/2$, $\beta=h_t/(H-d_b)$, H is story height, and d_b is the depth of the beam cross section.

Based on previous research findings [25], the panel zone undergoes yielding in a sequence that starts at the center and spreads outward to the surrounding area. If the bearing capacity is sufficient, the axial force in the column is completely transmitted to the column flange and the bolted end-plate connection of the semi-rigid joint [26]. Adopting a consistent distribution of shear stress simplifies the formulation and provides design results that are adequately sufficient.

In the following sections, following a general description of the employed AI algorithms in Section 3, a comprehensive database is created in Section 4 using a Finite Element approach. The shear strength of the panel zone for all samples is calculated using Eq. (5). This database forms the basis for the analysis carried out in Sections 5 and 6, where ML methodologies are used to evaluate and interpret the findings.

3. Applied artifactual intelligence algorithms

In this investigation, the ML models were created using the Scikit-learn ML package [44]. A total of twelve ML models were implemented including the following: KRR, PR, DT, RF, ETR, KNN, GB, XGB, LGBM, CatBoost, HistGB, and SVR.

The reason of selecting various ML models in this study can be explained by the general recommendation approach used in the ML methodologies, according to which, it is necessary to try different algorithms to find the one that would be the most suitable for solving the considered problem. Each problem shows different characteristics which might be more compatible with specific algorithms than others, and hence, this broad approach is applied in this study. Therefore, through the use of these models this study not only allows for the evaluation of the considered ML models' effectiveness, but also prevents the possibility of bias toward any particular model and ensures that the most appropriate model is used, depending on the set performance measures. This approach is further justified by the fact that these twelve models are well known and commonly used in the literature, thus validating their applicability across different fields of structural engineering [27]. Moreover, the use of SHAP algorithm enhances the interpretability of these models, hence providing the importance of different features for the model prediction, which is vital in understanding the mechanical behavior of connections. Understanding which features are most influential in the model's predictions allows for a deeper analysis and understanding of the underlying phenomena, thereby adding more value to the study. Discussing this subject in detail will result in an excessive length of the current study. Furthermore, there has been a recent publication of a review article [27] on the application of these algorithms in structural engineering as well as the examples of the use of these algorithms in different sectors of structural engineering. Consequently, to maintain the focus and conciseness of this study, only a brief overview of each algorithm is provided in the following sections.

3.1. Kernel Ridge Regression

Kernel Ridge Regression (KRR) is an advanced ML technique which is suitable for analyzing intricate data and especially when non-linearity is involved. As a combination of ridge regression with kernel methods, KRR provides a reliable tool for revealing complex relationships in the data. Ridge regression aims to prevent overfitting by adding a penalty term to the loss function, which shrinks the regression coefficients [45]. KRR follows this process with kernel functions that enable the modeling of non-linear relationship between the variables. The general idea of KRR is the projection of the given input data into a higher-dimensional feature space with the help of kernel function. The choice of kernel depends on the nature of the data and the specific problem being addressed [45].

3.2. Polynomial Regression

Polynomial Regression (PR) is an extension of the linear regression that utilizes polynomial functions of the input variables to model complex nonlinear relationship between the input parameters and the target response. PR is good at fitting complex and non-linear data. However, PR can be very sensitive to overfitting, especially if high degree polynomials are used [46]. The overfitting can be minimized by finding the appropriate degree of the polynomial through cross validation, thereby improving the model's performance on new data. Bagging, or Bootstrap Aggregating, increases PR's stability by training the model on different bootstrapped samples of the dataset and averaging the results [47]. The model complexity must be managed, and methods like regularization and feature scaling should be employed to enhance the utilization of PR without encountering numerical problems and overfitting.

3.3. Decision Tree

Decision Tree (DT) relies on criteria and starts with a root node as a representation of the whole dataset. In each cycle, the model evaluates all the current conditions and splits the samples into different nodes based on those conditions. The model divides the data into subgroups and creates new nodes and branches as the model progresses through the selected criteria [48]. The process of splitting or branching is repeated until the end points are pure in terms of classes or until other criteria is met, such as the minimum number of instances per node or the depth of the tree. The terminal nodes represent the forecast produced by the model. When applied to regression, each of the leaves pertains to a single value. The path from the root node to an end point represents a chain of choices that produce a given result [49].

3.4. Random forest

Random forest (RF) is an ensemble technique in the ML family that is used for improving the prediction reliability and accuracy by using a set of decision trees. This approach is efficient, as it takes advantage of a single DT algorithm while avoiding it's weaknesses. By using this approach, every tree learns from a randomly chosen subset of the training dataset, and a randomly chosen subset of features, thus diversity is incorporated into the model's predictions [50]. The data is randomly split into different sets using the bootstrapping method. This means that each tree is exposed to slightly different data, hence reducing the overfitting of the data. RF is produce by growing different decision trees in parallel with each other, and each tree making a different decision. In regression problems, the final prediction can often be the average of the outputs derived from the trees. The integration of multiple models results in the reduction of variance, hence leading to more stable and reliable predictions on unknown data [51]. Moreover, the process of randomly selecting a subset of features at each split point in the trees ensures that no single feature has excessive influence on the model. This increases the general variety and reduces the risk of overtraining.

3.5. Extra Trees Regression

The Extra Trees Regressor (ETR) is a ML algorithm that is based on the RF model, designed to perform regression with higher effectiveness and precision. In Extra trees multiple randomized decision trees are fitted on different samples of the dataset. This method uses the concept of ensemble averaging to increase the predictive power and reduce over fitting. Compared to conventional decision trees, ETR fully randomizes both the split points and features at each split, which results in higher variance reduction. Each tree in the ETR forest chooses the feature and split point randomly, rather than opting for the optimal split as in traditional decision trees. Additionally, each tree is grown on the entire dataset, not on bootstrap samples. This method, proposed by Geurts et al. [52], is quite suitable for dealing with large datasets and modelling nonlinear interactions between variables. The extreme randomness in the splitting process results in highly diverse trees, which, when combined, help in lowering the chances of overfitting and bias. The important parameters in ETR include the number of trees, number of features that are randomly selected in each split, the minimum sample size per split. Therefore, ETR is a stable solution for regression problems because it is fast and does not require significant hyperparameter optimization.

3.6. K-Nearest Neighbors

The basic principle of operation of K-Nearest Neighbors (KNN) is to use distance metrics between data points in the feature space to make predictions. KNN uses the (k) nearest data points in the training set, where (k) is a predetermined number, to make predictions for a new data point. In regression problems, the KNN algorithm calculates the average of the value of the k nearest neighbors of a new data point [53]. In this regard, the predicted result is influenced by the values of the neighboring points leading to a forecast that reflects the characteristics of the local neighborhood. The performance of KNN relies on the value of (k) and the distance measure used to determine the proximity of samples. Common distance metrics include the Euclidean distance, the Manhattan distance, and the Minkowski distance. The parameter (k) determines the level of localization of the decision boundary. Lower values of (k) can capture finer details of the data but are vulnerable to noise while higher values enable more generalized predictions. Thus, choosing an appropriate (k) value is important for balancing detail and generalization in the model's predictions. KNN is an easy and understandable algorithm, but it can be slow and time-consuming, especially when it is used on large data sets [53]. However, KNN is still widely applied because its ease of calculation and higher accuracy in cases where the relationship between features and the output variable is complex and not easily modeled by parametric equations.

3.7. Gradient Boosting

Gradient Boosting (GB) is executed by successive steps of minimizing the loss function which could be mean square error [54]. The following steps may be used to apply this technique. First, a simple model, for example, a decision tree with limited depth, is trained on the given dataset. This first model is known as the basic learner. Then, the residual errors which are the differences between the predicted values and the actual values are calculated. In the subsequent stages, new models are trained in order to predict such deviations. Every new model is an attempt to correct the errors of previous models. The forecasts produced by these new models are combined with the forecast of the earlier models to form an improved model. This is repeated for a certain number of iterations or until the residuals reach a certain level of tolerance. In Gradient Boosting the term 'gradient' refers to the gradient descent method that is used to optimize the loss function. In each step of the loop, the method calculates the gradient of the loss function with respect to the model's predictions and adjusts the parameters. Thus, the approach effectively decreases the model's prediction error [54].

3.8. Extreme Gradient Boosting

Extreme Gradient Boosting (XGBoost) is a Boosting method which is derived from GB ML framework. It is used for its efficiency and effectiveness especially in terms of its predicted accuracy. Unlike the gradient descent method that involves adjusting all the parameters over the whole dataset, XGBoost improves the model gradually by adding more trees that focus on the mispredictions made by the previous trees. In each of these processes, it uses gradient descent to effectively optimize a specific loss function [55]. Moreover, XGBoost has several additional elements that can improve the model's efficiency; for instance, overfitting prevention techniques, parallel tree growth for faster processing, and the ability to handle sparse data [55].

3.9. Light Gradient Boosting Machine

Light Gradient Boosting Machine (LGBM) is developed using the GB technique. LGBM's speed and performance are enhanced by two key algorithms: Gradient-based One-Side Sampling (GOSS) and Exclusive Feature Bundling (EFB) [53]. This way, GOSS enhances the training process as it directs LGBM to focus on the most informative samples. This is accomplished by prioritizing cases with large gradients, as these cases are more likely to improve the model's accuracy. Additionally, a subset of the less significant cases (with smaller gradients) is randomly sampled, ensuring that the model captures a wide range of data points while focusing on the most informative ones. Thus, the training process is carried out much faster, hence reducing the volume of data that has to be trained. Exclusive Feature Bundling (EFB) aims at decreasing the data size by combining mutually exclusive features, which are features that rarely take non-zero values simultaneously. Reducing the feature space is a realistic method that helps LGBM manage large datasets. LGBM utilizes the leaf-wise tree construction procedure rather than the level-wise one, which is used in most traditional boosting methods. LGBM constructs trees by sequentially adding leaves in a manner that maximizes loss reduction at each stage [56].

3.10. Categorical boosting

Categorical boosting (CatBoost) is a GB based method that is similar to XGBoost and LGBM. But it is more advanced in terms of the handling of categorical data. The system is particularly designed to provide an efficient computation of the categorical variables by utilizing a strategy that incorporates target statistics. This technique is beneficial in reducing the problem of leakage and overfitting, which is usually associated with normal encoding. CatBoost uses an ordered boosting approach which makes the model more stable and accurate [57].

3.11. Histogram-Based Gradient Boosting

Histogram-Based Gradient Boosting (HBGB) is a more developed form of the ML method called Gradient Boosting Decision Trees (GBDT). It does this by discretizing continuous features into bins and creating histograms that reduce the time and memory needed for training. This method is faster since it searches for the best splits in fewer candidate points. In each decision tree of the ensemble, the errors of previous trees are corrected through gradient descent on the loss function [58]. Compared to other models, HBGB has a natural ability to address categorical features and missing values by setting them to bins, which improves its flexibility. It is most useful when dealing with large data and those with numerous features since it is less sensitive to issues of data distribution and outliers. In addition, HBGB is highly scalable due to its ability to parallelize its operations and is suitable for modern data-intensive applications [58].

3.12. Support Vector Regressor

Support Vector Regressor (SVR) is a type of ML technique derived from the support vector machine (SVM) for those problems where the dependent variable is a continuous variable [57]. It seeks to identify a function deviate from observed values by no more than epsilon (ε), and at the same time minimizing the model complexity while maximizing the prediction accuracy using convex optimization. The technique of SVR involves mapping of the input data into a higher-dimensional feature space using kernel functions to perform linear regression in this space. The method is less prone to overfitting and does not depend on the distribution of the data. Among the hyperparameters which have a higher impact on the SVR, there are the capacity value (C), epsilon (ε) and the kernel type. Some of the most widely used kernel functions are linear kernel, polynomial kernel, radial basis function (RBF) kernel, and Sigmoid kernel [57]. Other hyperparameters are generally set by optimization techniques such as particle swarm optimization, Bayesian optimization, and grid search for better performance of SVR. because of such flexibility and stability, SVR is used in many fields as one of the most popular techniques.

3.13. SHapley Additive exPlanations (SHAP) algorithm

In the context of ML systems, explainability can be defined as the ability to explain or to present a parameter in a format that can be easily understood by a human. Explainability is the measure of how well a ML model can justify its reasoning for a given prediction or decision and particularly can be measured by how well a human can comprehend the model's decision-making process. SHAP model-agnostic explanation [59], can be chosen as one of the well-known methods in the field of XAI. SHAP, an explanation framework for the various ML models, which is based on the Shapley value and game and probability theory [59]. As part of the model decision-making process, SHAP uses both the global and local measurements. This way, the relationship between the model's features and the output targets can be identified and thus the behavior of

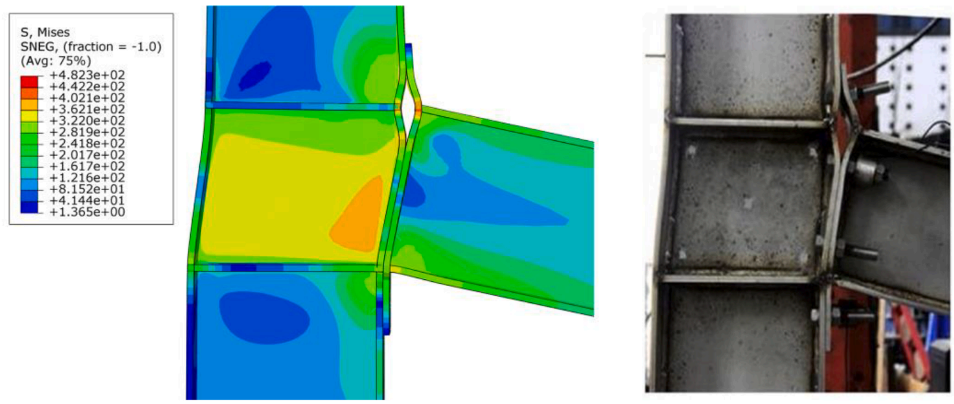

Simplified Shell model-specimen 1 **Test- Specimen1 (Gao et al.) [64]**

(a)

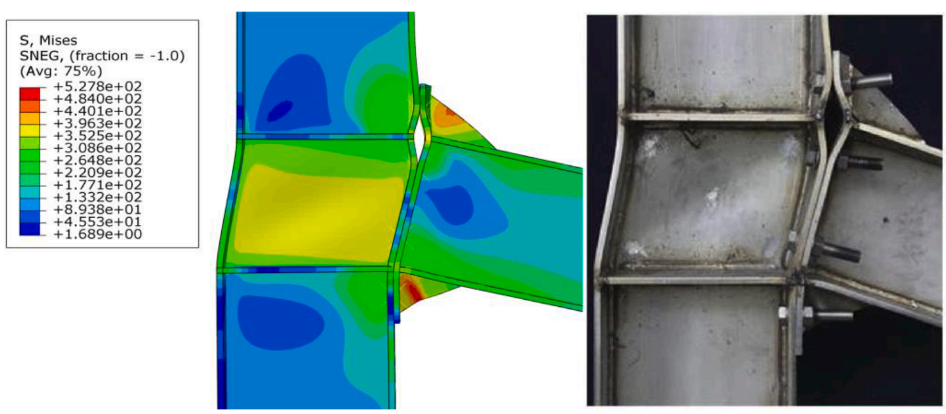

Simplified Shell model-specimen 2 **Test- specimen2 (Gao et al.) [64]**

(b)

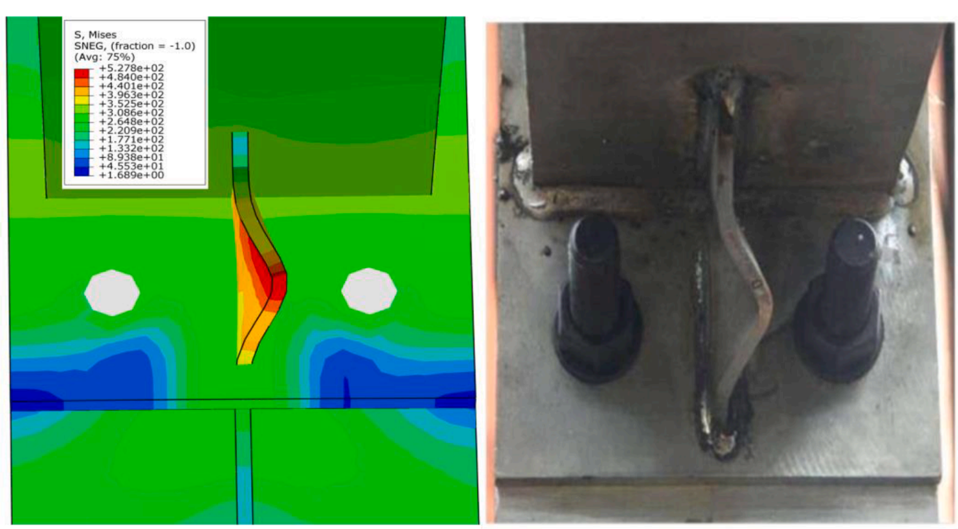

Buckling of compression rib stiffener-specimen 2 **Test- specimen 2 (Gao et al.) [64]**

(c)

Fig. 3. (Simplified shell models are displayed using rendering shell thickness feature): Comparison of numerical and experimental failure modes.

the model can be explained. Shapley's Additive Explanation has been beneficial by identifying the precise weights of features for a specific prediction. The theoretical construct identifies model with game rules and features with players who may be present in the game and absent. In this metaphor, Shapley values are obtained from the evaluation of the model by different subsets of the input variables. By understanding the

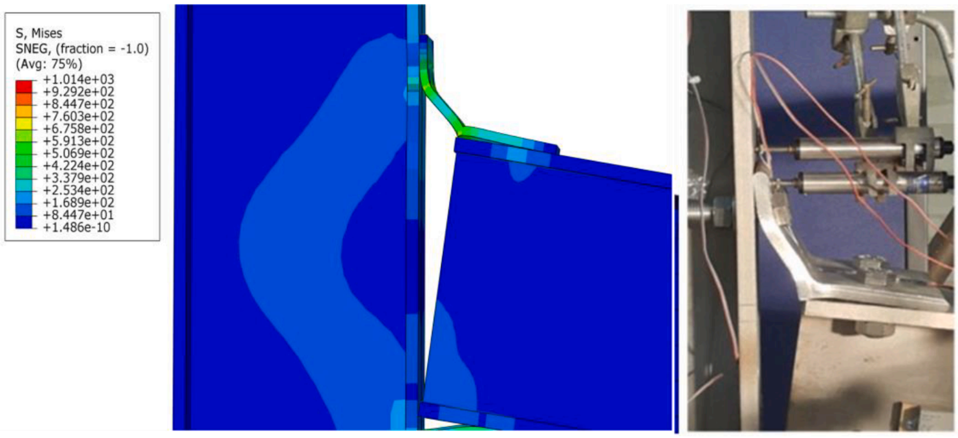

Simplified Shell model-specimen 3 **Test- specimen 3 (Elfah et al.) [65]**

(d)

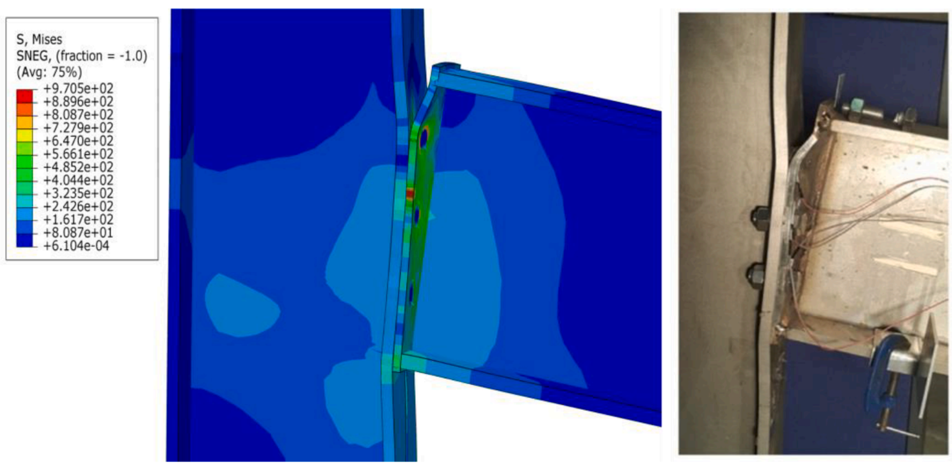

Simplified Shell model-specimen 4 **Test- specimen 4 (Elfah et al.) [65]**

(e)

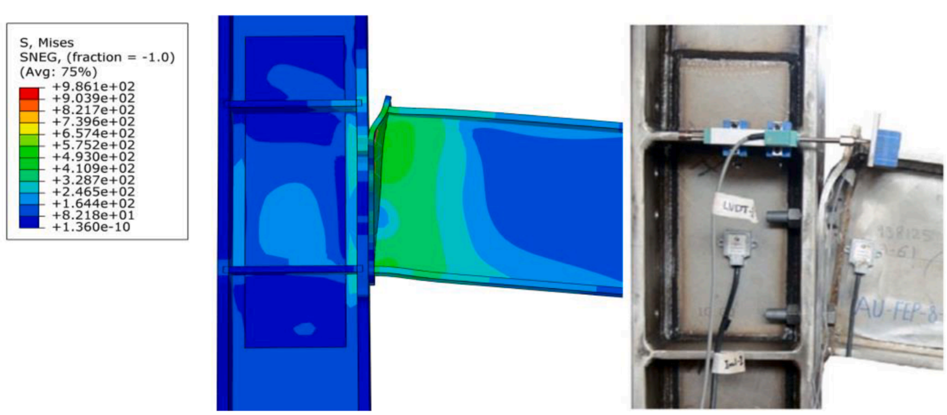

Simplified Shell model-specimen 5 **Test- specimen 5 (Song et al.) [66]**

(f)

Fig. 3. (*continued*).

relationship between the model's features and output targets, it is possible to interpret the behavior of the model.

4. Finite Element modeling and validation

This study relied on FE analysis as an essential step of the database development, because experimental data on stainless-steel column web

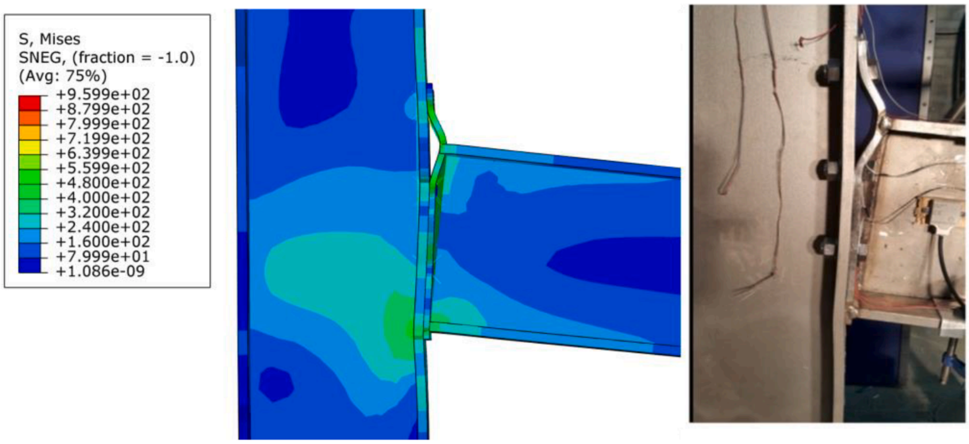

Simplified Shell model-specimen 6 **Test- specimen 6 (Elfah et al.) [65]**

(g)

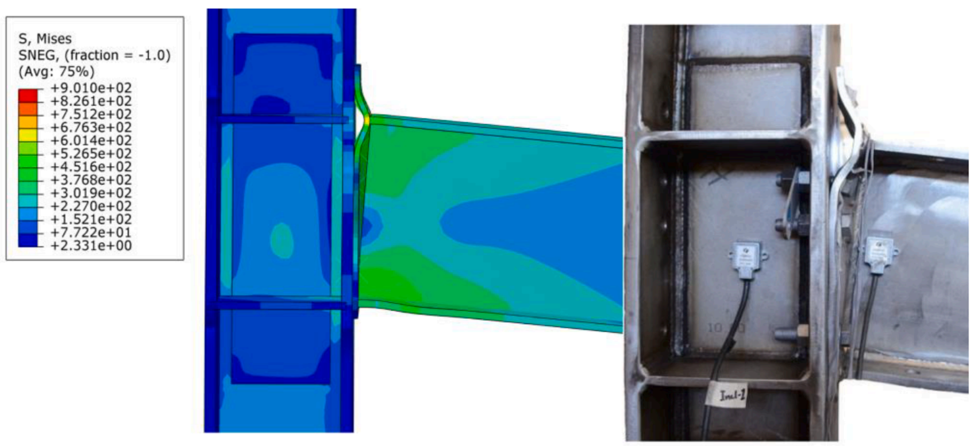

Simplified Shell model-specimen 7 **Test- specimen 7 (Song et al.) [66]**

(h)

Fig. 3. (*continued*).

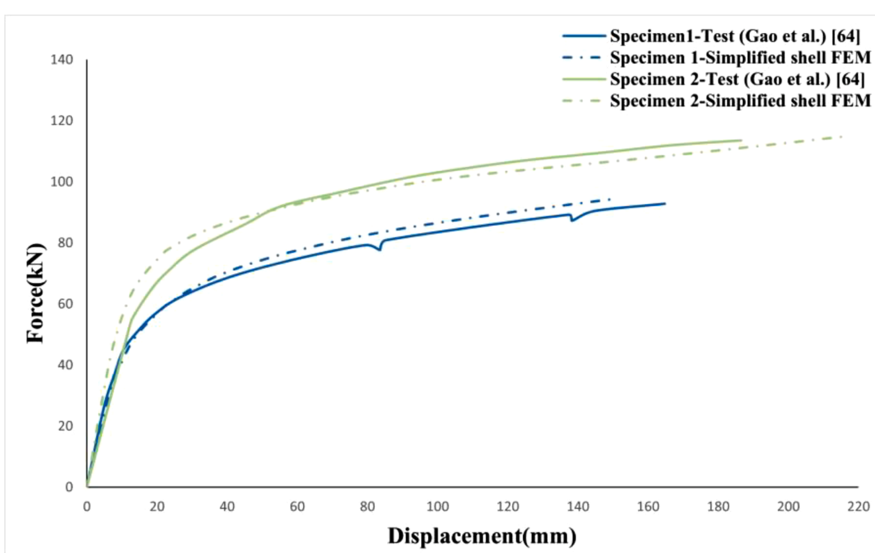

Fig. 4. force-displacement curves for specimens (1–2).

Table 1
Comparison between FE and test results for specimens (1–2).

Specimen	FE / Experimental results			
	$K_{j,ini}$	$F_{j,R}$	$F_{j,u}$	$\Delta_{j,u}$
Specimen 1	0.92	0.98	1.02	0.91
Specimen 2	1.19	0.97	1.02	1.15
Average	1.05	0.97	1.02	1.03
St.dev	0.135	0.005	0.0	0.12

Table 2
Comparison between FE and test results for specimens (3–7).

Specimen	FE / Experimental results			
	$S_{j,ini}$	$M_{j,R}$	$M_{j,max}$	$\Phi_{j,u}$
Specimen 3	1.08	0.96	1.05	1.04
Specimen 4	0.96	0.95	0.97	1.02
Specimen 5	0.96	1.09	1.05	1.06
Specimen 6	1.03	0.96	1.05	1.01
Specimen 7	0.85	1.09	1.05	1.06
Average	0.976	1.01	1.034	1.038
St.dev	0.078	0.065	0.032	0.020

panels are limited. By the development and validation of the 3D nonlinear FE model, a large database of configuration conditions was obtained. This database was used as the basis for training the ML models employed in this study to provide accurate estimates of shear strength.

In previous studies conducted by current authors [10,60], a 3D nonlinear FE model was developed in Abaqus [43] to analysis the behavior of various connections for which experimental test data were available. Building on that FE model, this paper presents and validates a numerical modeling procedure for the connections at hand. The ABAQUS scripting interface with Python [43] then used the validated numerical model to generate a large dataset automatically through loop creation. An overview of the FE modeling used in the study is provided in the following. The material behavior of stainless-steel was described by the nonlinear relationship suggested by Rasmussen [61]. This relationship holds that the material yield surface grows uniformly in the stress space as the plastic strains increase, which is called isotropic hardening. In this study, the mechanical properties of austenitic stainless-steel, such as yield strength and elastic modulus, were adopted based on the recommendations provided in Eurocode 3 Part 1–4 (EN 1993–1–4) [13]. For detailed values and guidelines, readers are encouraged to refer to the Eurocode document [13]. In the FE model, quadrilateral 4-node shell elements known as S4R elements were used. In this case, in order to correctly record the panel zone deformations, at least five elements were used across the thickness of the plate. By performing a mesh sensitivity analysis, the mesh sizes varying from 5 mm to 40 mm were evaluated. Then, a structured mesh in various sizes was used. A finer mesh size of 5 mm was applied in areas of the model considered to be subjected to concentrated loads, while the rest of the model was meshed with a larger size of 20mm. Only the horizontal displacements at the cross section of the upper part of the column were restrained, whereas, all the degrees of freedom at the bottom section of the column were restricted. At the beam end, where out-of-plane displacements were also limited, a monotonic load was applied. To model the bolts, a simpler approach was taken; they were modeled with the help of an Abaqus cartesian connector element. To characterize the element, it can be defined as a spring with the elastic-plastic failure behavior in axial as well as shear mode. Compared to solid elements, these elements are considerably more efficient in terms of computational requirements. More specifically, it has been found in prior studies that using this approach to model bolts is effective [57,62,63]. The circular-shaped "rigid body" was incorporated into the model to ensure that any undesired deformation that may occur in the connector region is avoided. The tangential behavior was described using the penalty friction coefficient which was assigned as 0.3. The hard contact option

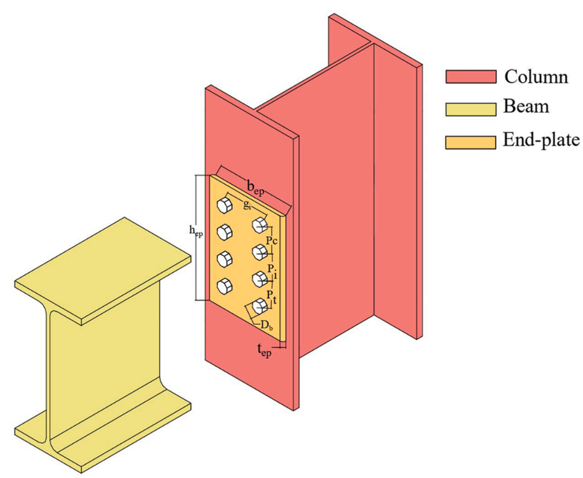

Fig. 6. General description of input features.

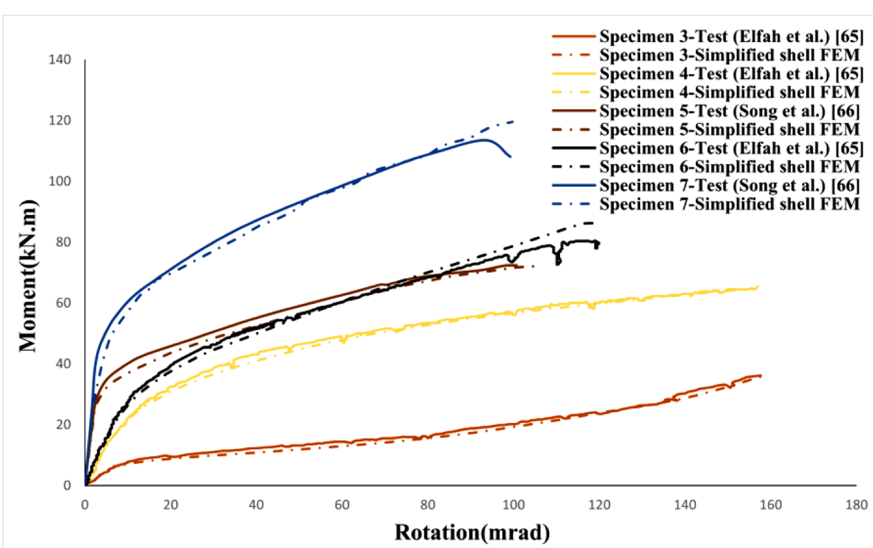

Fig. 5. moment-rotation curves for specimens (3–7).

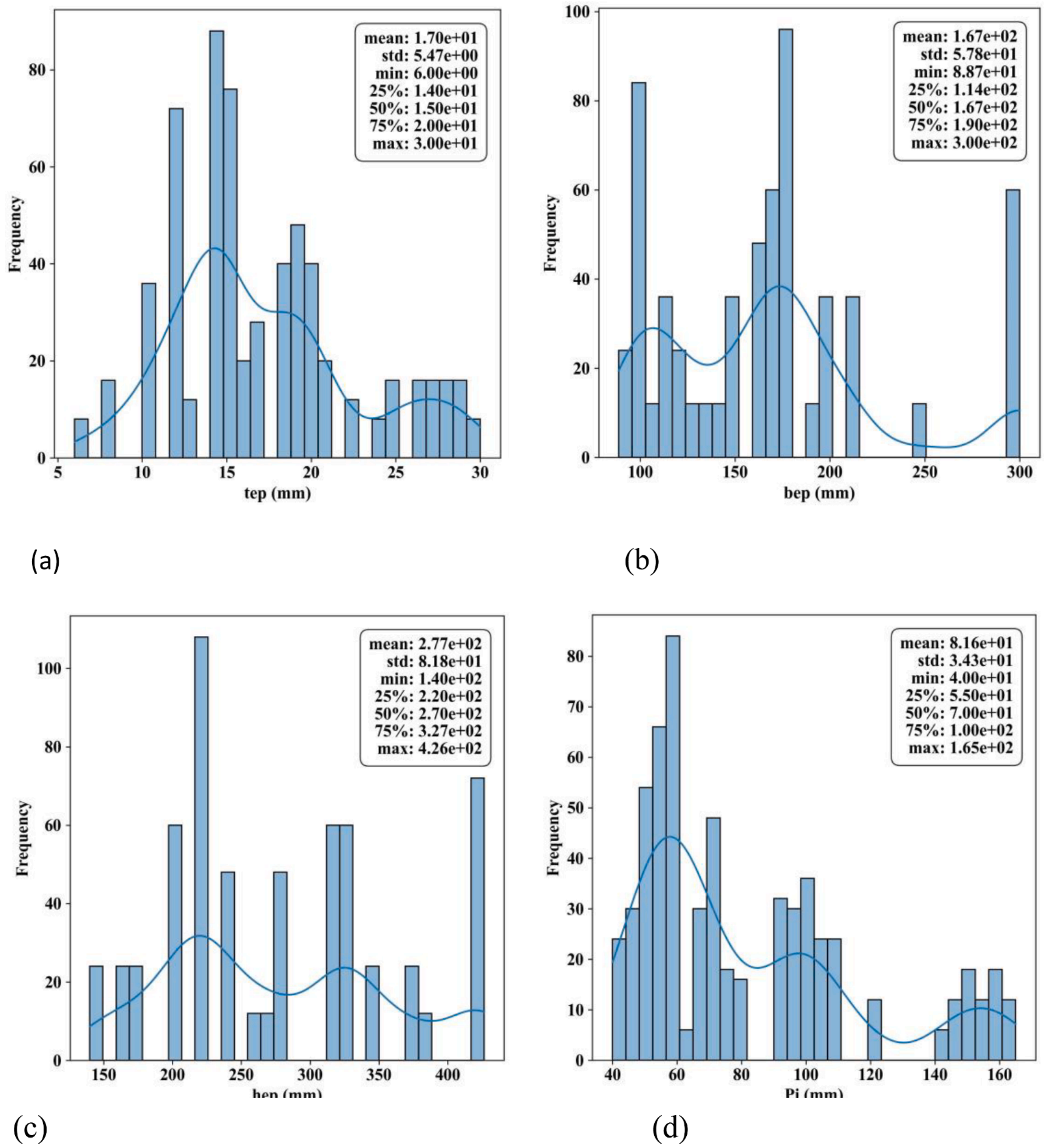

Fig. 7. The distribution of effective input features.

was chosen in order to permit a potential separation following contact. In the simulations, the main-secondary surfaces technique was used for modeling plate contacts using Abaqus software[43]. To validate the implemented finite element modeling procedure, the results were compared with available experimental data for seven different types of beam-to-column connections made of stainless-steel from three separate experimental studies [64–66]. Fig. 3 illustrates the failure mechanism that occurs during deformation under the highest load.

Fig. 3(a–f) shows that the numerical failure modes match the experimentally observed failure modes. In addition, it is evident from Fig. 3(a–f) that the FE prediction of connector failure matches the failure observed in the experiment that validates the connector failure definition used in the model. These models depicted a large scale of plastic deformations akin to those observed in the column flange and end-plate of the FE models. As shown in Fig. 3(g and h), there was a consistent deformation in a t-stub of the specimens. In this pattern, the tension flange of the beam and the end plate between two bolt rows came under tension. The proposed model captured this behavior effectively. Furthermore, the model accurately replicated the specific bending of the column flange. The finite element results agreed well with the test data, which means that the finite element models can accurately describe the performance of beam-to-column joints.

Figs. (4 and 5) show a comparison of the force-displacement curves for specimens (1–2) and the moment-rotation curves for specimens (3–7).

To compare the numerical predictions by FE analysis with the experimental data, the primary joint characteristics reported in Tables 1 and 2 were used. Since the load-displacement results for the first two specimens were provided by the reference test [64], these were extracted from the FE analysis and the comparison results are shown in Table 1. Similarly, for specimens 3 to 7, where moment-rotation curves were provided by the reference tests [65,66], the corresponding moment-rotation characteristics were obtained from the FE analysis and the comparison results are presented in Table 2. Table 1 shows the plastic resistance (F_{Rd}), initial stiffness ($K_{j,ini}$), ultimate resistance ($F_{j,u}$), and ultimate deformation ($\Delta_{j,u}$) comparison results. Table 2 presents the

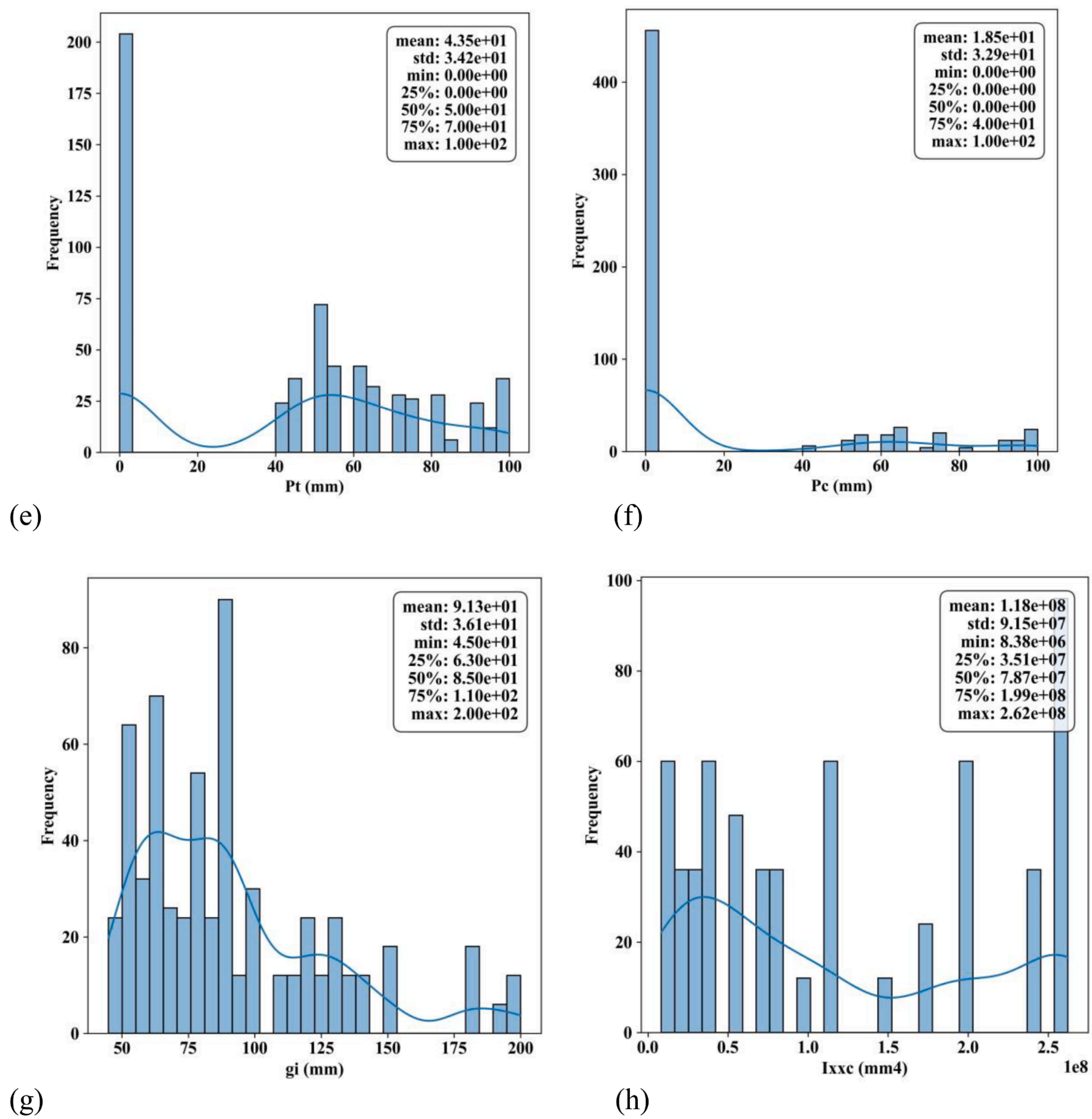

Fig. 7. (*continued*).

plastic moment resistance ($M_{j,R}$), initial rotational stiffness ($S_{j,ini}$), maximum moment capacity ($M_{j,max}$), and ultimate rotational capacity ($\Phi_{j,u}$) comparison results of the joints.

The average ratios of $K_{j,ini}$ (derived from the slope of the force-displacement curve) and $S_{j,ini}$ (obtained from the slope of the moment-rotation curve) are 1.05 and 0.976, respectively, with standard deviations of 0.135 and 0.078, which shows that the FE models have slight differences in predicting these stiffness values. Plastic resistance (F_{Rd}), determined by the intersection of the initial stiffness ($K_{j,ini}$) line with the tangent line of the hardening part of the load displacement curve, and plastic moment resistance ($M_{j,R}$), determined by the intersection of the initial rotational stiffness ($S_{j,ini}$) line with the tangent line of the hardening part of the moment rotation curve, are measures of the load and moment at which the connection transitions from elastic to plastic behavior. The average ratio for F_{Rd} is 0.97 with a standard deviation of 0.005, indicating that the FE models have a good agreement with minimal variation from experimental data. The average ratio for $M_{j,R}$ is 1.01 with the standard deviation of 0.065, which in general shows an accurate prediction of plastic moment resistance by the FE models.

Ultimate resistance ($F_{j,u}$) and maximum moment capacity ($M_{j,max}$) define the peak load and moment the connection can sustain before failure. The FE models show strong alignment with experimental results, as indicated by an average ratio of 1.02 for $F_{j,u}$ (standard deviation 0.0) and 1.034 for $M_{j,max}$ (standard deviation 0.032). These results suggest that the FE models reliably predict the connection's maximum capacity. Ultimate deformation ($\Delta_{j,u}$) and ultimate rotational capacity ($\Phi_{j,u}$) are parameters that define ductility of the connection and its capacity to undergo large deformations before failure. The FE models slightly overestimate these values, with average ratios of 1.03 (standard deviation 0.12) for $\Delta_{j,u}$ and 1.038 (standard deviation 0.020) for $\Phi_{j,u}$. However, the low standard deviations indicate consistent predictions across specimens.

From Figs. (3–5) and the numerical values given in Tables (1 and 2) it is possible to conclude that there is a very good agreement between the numerical model and the experimental data. The developed FE models are able to capture the structural response of all the considered

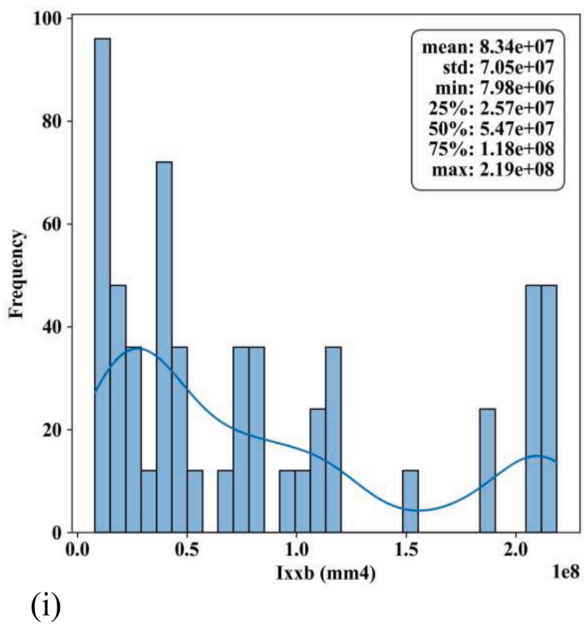

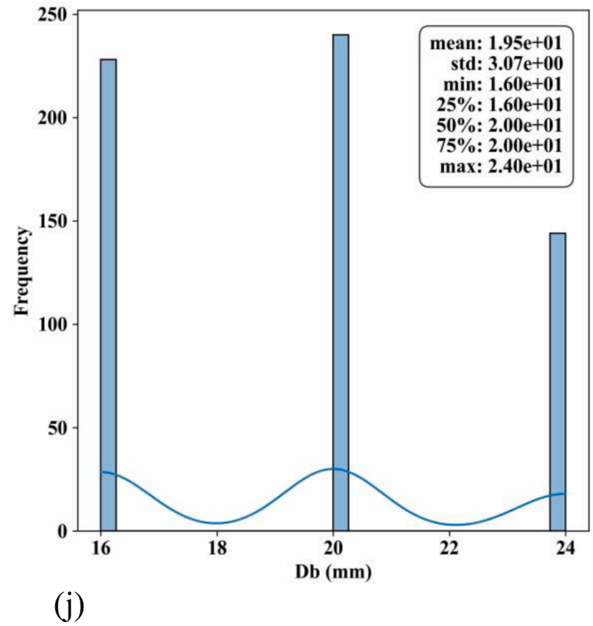

Fig. 7. (*continued*).

specimens and are therefore utilized to develop the database.

5. ML model development and configuration

5.1. Statistical analysis of the compiled database

The British Stainless-steel Association has published a comprehensive list of stainless-steel sections [67]. According to this list, in the initial phase, all the stainless-steel sections that were accessible were identified, resulting in a total of 150 H-shaped column and welded I-shaped beam sections from various suppliers. Nevertheless, it is not feasible to consider every conceivable arrangement of these segments. Thus, only a limited number of connections that meet the specific criteria of the design guidelines were meticulously taken into account for this study. Finally, after implementing these restrictions and practical guidelines for connection setup, a total of 612 samples were deemed suitable for analysis. Fig. 6 shows a general description of input features.

Fig. 7 depicts the statistical distribution of the 10 considered input features including: the bolt diameter (D_b), the end-plate width (b_{ep}), the end-plate height (h_{ep}), the end-plate thickness (t_{ep}), the bolt spacing in tension (P_t), the bolt spacing between comparison bolts (P_c), the horizontal distance between bolts (g_i), and the vertical distance between the innermost tension bolt and the innermost comparison bolt (P_i), the column and beam second moment of inertia (I^c_{xx}, I^b_{xx}) where frequency indicating the number of samples in the database. Fig. 8 illustrates the impact of each parameter. The intensity of the color increases proportionally with the frequency of the input parameters falling inside this range. From Figs. (7 and 8) the following results are evidence: the t_{ep} values are ranged between 5 mm and 30 mm with the most frequency in the 10–20 mm range. In this range V_{pz} shows higher values. The b_{ep} values range from 88.7 mm to 300 mm, with most of the data points located at 100–150 mm and 200–250 mm ranges. Fig. 8 shows that V_{pz} values increase with higher b_{ep}, particularly concentrated around 150–200 mm. The h_{ep} values range from 140 mm to 426 mm, with significant data concentration around 200 mm, 300 mm, and 400 mm. Fig. 8 shows V_{pz} increasing with higher h_{ep} values, particularly around these concentrations, which are within typical ranges used in practice. The P_c values show a strong clustering around 0 mm with fluctuations that can rise up to 100 mm. In fact, the zero values of P_c indicate that the connections have a single row of compression bolts. Fig. 8 also depicts that V_{pz} is higher at lower P_c values. The P_i values are between 40 mm and 160 mm with a relatively high density at 50 mm to 100 mm. Fig. 8 shows V_{pz} values are higher with increasing P_i, particularly around these concentrations. The P_t values show a strong clustering around 0 mm with occasional spikes up to 100 mm. Indeed, the zero values of P_t indicate that the connections possess only one row of tension bolts. For g_i, the values range from 45 mm to 200 mm, with most values between 50 mm and 110 mm, indicating a broad distribution. The I^b_{xx} values range from 7.98e+06 mm^4 to 2.19e+08 mm^4. Additionally, V_{pz} values are concentrated at lower I^b_{xx} values. Similarly, I^c_{xx} values range from 8.38e+06 mm^4 to 2.62e+08 mm^4, showing V_{pz} concentration at lower I^c_{xx} values. Lastly, the D_b values range from 16 mm to 24 mm, reflecting the use of only three bolt sizes: 16 mm, 20 mm, and 24 mm.

5.2. Data pre-processing

Before training and testing the ML models, data preparation was carried out. This process involved converting raw data into a format that made data more effective. The completion of this phase was important for achieving optimal model performance, because in case of failure of this step, the accuracy of the models could negatively affected. Therefore, before training the ML models on the acquired dataset, the data needed to be preprocessed and structured appropriately using the feature scaling. The values of the independent features are scaled with the help of the min-max scaler (Eq.6) which is a mathematical technique that normalizes the input characteristics to a range between (−1 and 1). This is necessary because the independent features characterize various quantitative measures and dimensions. The objective is to adjust the size of both input characteristics and output values to fit into a different range, in order to avoid the dominance of bigger numerical values over smaller ones [27].

As part of this data preparation process, statistical analyses were conducted to verify data quality and completeness. Checks for missing values confirmed that the dataset was complete, with no missing values identified. Additionally, outlier detection was performed, confirming that all data points were within acceptable ranges. Subsequently, the database that had been prepared and scaled was randomly partitioned into two distinct subsets: a training set and a test set. One of the widely used strategies when building multiple machine learning models is to

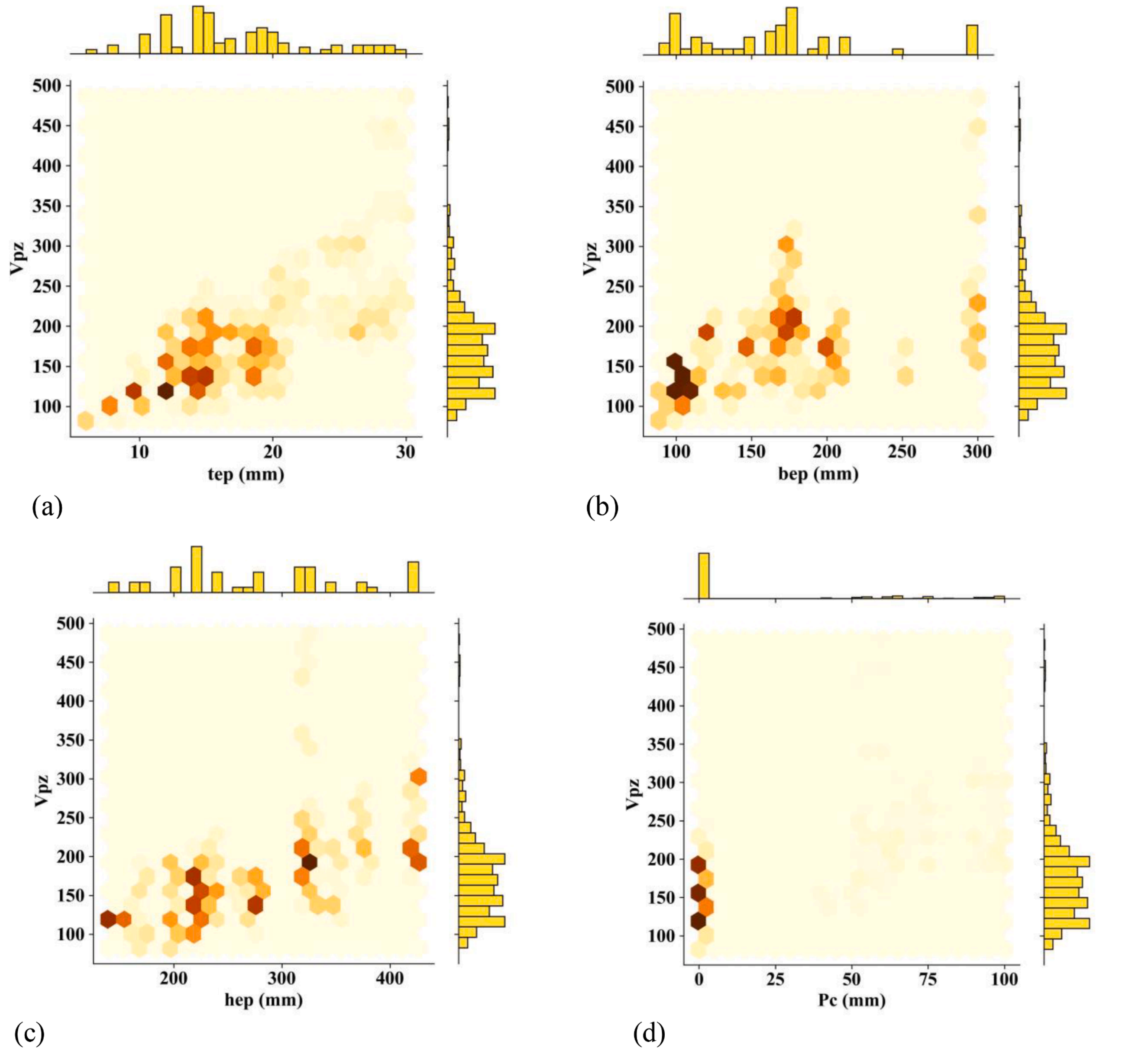

Fig. 8. Hexagonal contour graph of the input and output parameters in the database.

split the data in the following way: 80 % of the data can be used for the training set while only 20 % of the data can be used for the testing set. The testing set was kept unseen and was used solely for the verification of the model's accuracy without being employed for training purposes. Fig. 9 shows the general approach utilized for training ML models.

$$x_n = \frac{2(x - x_{\min})}{(x_{\max} - x_{\min})} - 1 \tag{6}$$

5.3. Performance evaluation of modeling

To evaluate the performance of the ML models in this study, three different statistical metrics were used. The calculation of the Coefficient of Determination (R^2) determines the extent to which the independent variable(s) predict the variance in the dependent variable (Eq. 7.a). The Root Mean Square Error (RMSE) quantifies the average magnitude of errors between predicted and actual values, providing an indication of the typical deviation of predicted values from the actual values. The calculation assigns greater importance to larger errors and is determined by taking the square root of the average squared difference between predicted and actual values (Eq. 7.b). The Mean Absolute Error (MAE) is a metric used to evaluate the precision of a predictive model. It is calculated by taking the average of the absolute differences between the predicted values and the actual data, as shown in (Eq. 7.c).

$$R^2 = 1 - \frac{\sum_{i=1}^{n} (V_i - \widehat{V}_i)^2}{\sum_{i=1}^{n} (V_i - \overline{V})^2} \tag{7.a}$$

$$RMSE = \sqrt{\frac{1}{n} \sum_{i=1}^{n} (V_i - \widehat{V}_i)^2} \tag{7.b}$$

$$MAE = \frac{1}{n} \sum_{i=1}^{n} |V_i - \widehat{V}_i| \tag{7.c}$$

$V_i$is the actual value, $\widehat{V}$is the predicted value,$\overline{V}$is the mean of actual values, and n is the number of observations.

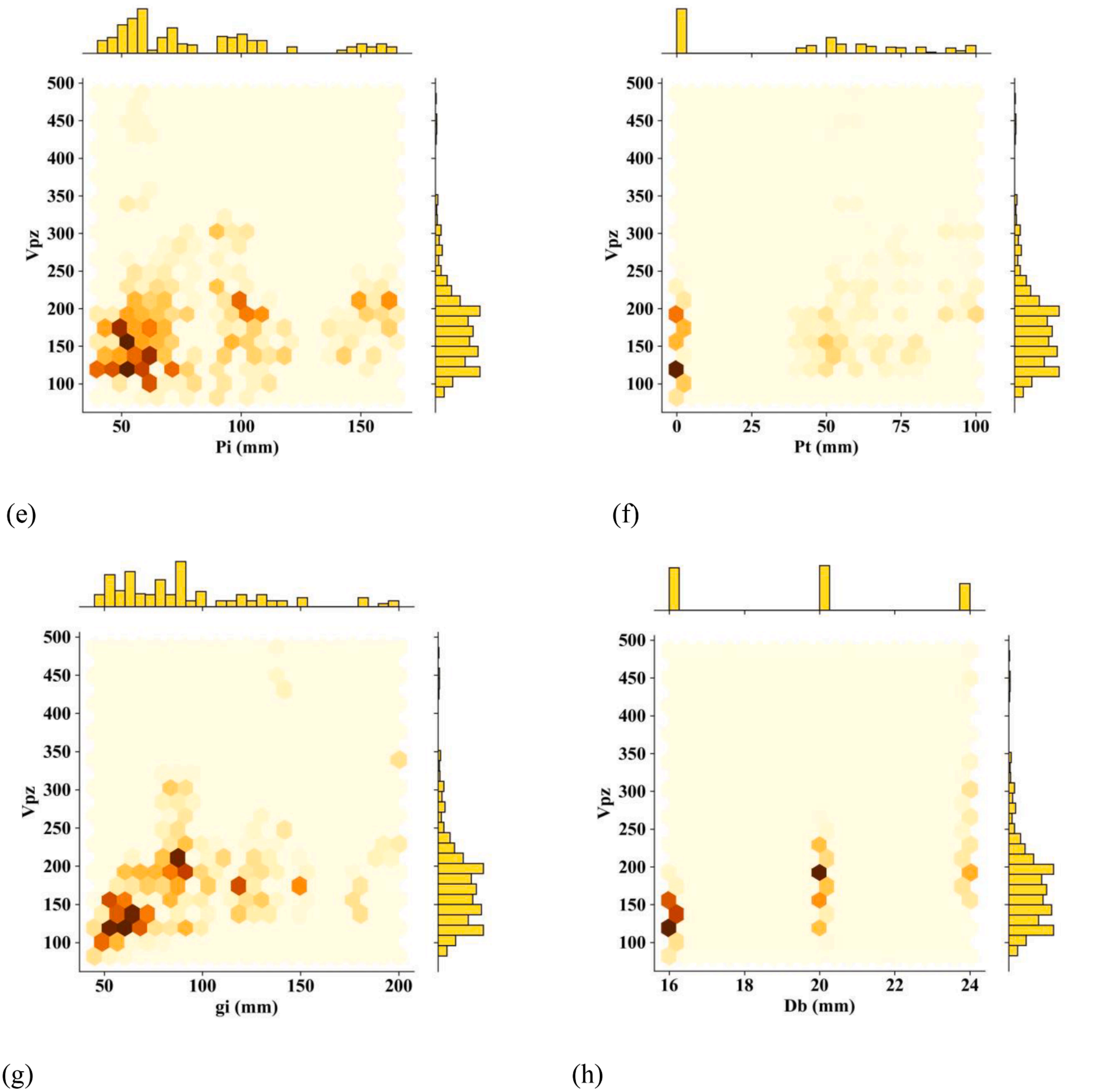

Fig. 8. (*continued*).

5.4. Model training and hyperparameter optimization

With regard to the architecture of an ML model, hyperparameters are important as they dictate the behavior of the training process and are not changed as the model is trained. Choosing the right hyperparameters depends on the data and algorithms and the objectives of the problem at hand. To identify optimal hyperparameters, search algorithms are used to explore the hyperparameter space. These algorithms continue training the models with different parameters, then assess the accuracy of the models, and refine their choices until the most effective parameters are found. In this study, both the randomized as well as the grid search method was applied. First, random search selected random hyperparameters within certain ranges and performed the search. This was followed by a grid search whereby the study tested all possible combinations within these ranges. In an attempt to overcome overfitting, a 5 fold cross validation algorithm was used [44]. This was done by partitioning the training data into five equal partitions or folds, and iteratively using each fold as a validation set while the others served as the training set. The collection of hyperparameters that produced the best performance was selected after all possible combinations were assessed.

6. Results and discussions

6.1. Cross-validation scores results

Fig. 10(a) depicts the average MAE for different ML models, utilizing a 5-fold cross-validation approach. In each boxplot, the top and bottom of a box represents the interquartile range (IQR) and the middle horizontal line within a box represents the median. The whiskers extend to the last data points till 1.5 times the IQR, and the points that are below this lower limit or above the upper limit are considered to be outliers. As seen in the case of ETR model in Fig. 10(a), the median MAE is the lowest; it can be then concluded that in terms of minimizing the absolute

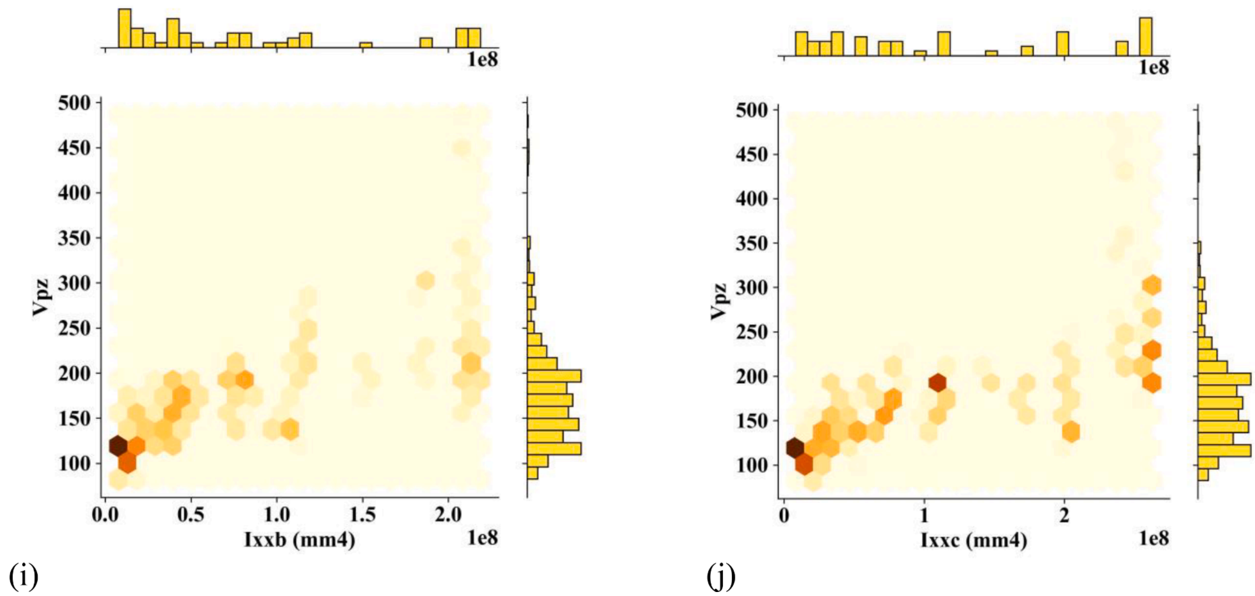

Fig. 8. (*continued*).

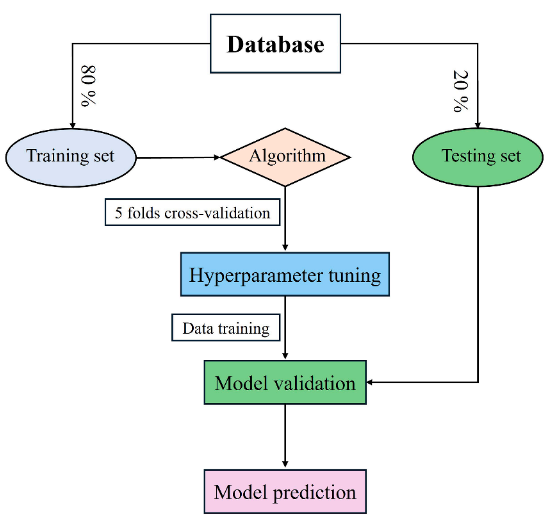

Fig. 9. General flowchart outlining the process of model generation for each model.

errors, ETR outperforms all the other models. Other methods such as HistGB, CatB, and GB also have low median of MAE which suggest that they are also performing well. On the other hand, SVR and PR have higher median MAE compared to the other models, which indicates poor performance. The IQR of the DT and KNN models are larger, which shows that their performance varies in different folds. Algorithms such as RF and LGBM show reasonable stability with low MAE values and narrow distribution.

The R^2 values are depicted in Fig. 10(b) and represent the extent of variance in the dependent variable accounted for by the models. It can be seen that higher R^2 values are indicative of a better model. ETR is once as the most accurate model with the highest median R^2 from Fig. 10 (b). Models like HistGB, CatBoost, and GB also have high median R^2 values, which proves the good quality of the models in terms of explanatory power. However, PR and SVR indicates lower Median R^2 which implies that they are less efficient in capturing the variation of the data. It can be seen that KRR and DT models have comparatively larger IQRs and few outliers suggesting that the models have more variation in their performance. The results for RF, LGBM, and XGB are highly accurate with narrow variations indicated by the R^2 values.

Fig. 10(c) depicts the RMSE values of the models. The smaller the RMSE value the better is the predictive accuracy of the model. ETR also demonstrated good results by having the lowest median of RMSE, which proves that this algorithm is reliable in minimizing the error of prediction. HistGB, CatBoost, and GB also demonstrate relatively low RMSE values, which points to the models' high accuracy. Other models such as SVR and PR have less accuracy as depicted by their higher RMSE. In terms of the model's performance, the DT model has the lowest accuracy and a large spread of scores with several outliers. RF and LightGBM show the stability of the model with relatively low RMSE values and a narrow range of distribution. KNN and KRR models provide a moderate level of accuracy with significant variation.

6.2. Machine learning model performance evaluation results

This study makes reference to statistical criteria, namely R^2, *RMSE*, and *MAE*, to assess the accuracy of ML models in predicting shear strength of stainless-steel panel zones. The comprehensive performance of these models, including training, testing, and all datasets, is presented in Table 3.

From Fig. 11 and Table 3, ETR and CatBoost are identified to be the best models for all the metrics and the datasets used. For the R^2 value, ETR has the highest with a value of 0.992 on the training set, and 0.968 on the testing set, shows that the model fits the data very well and has a very good predictive capability. It also maintains the least RMSE (5.057 on training and 10.306 on testing) and MAE (2.664 on training set and 7.196 on testing set), thus depicting the least prediction errors. This high performance is due to the fact that ETR is less prone to overfitting; since it uses an ensemble of decision trees where the average of the output of the trees is taken which improves both the accuracy and the generalization. CatBoost also gives very good results with R^2 values of (0.992 on training and 0.968 on testing), and RMSE (5.314 on training set and 10.217 on testing set), as well as MAE (3.426 on training set and 7.562 on testing set). CatBoost's gradient boosting algorithm helps in the proper optimization of the model by handling categorical features efficiently and reducing overfitting. HistGB and RF models are also identified to have good performance. HistGB results in an R^2 of (0.992, 0.964), with RMSE values of (5.072 and 10.842) and MAE values of (3.035 and 7.741) on training and testing sets, respectively. RF follows closely with R^2 values of (0.990, 0.964), RMSE of (5.793 and 10.777),

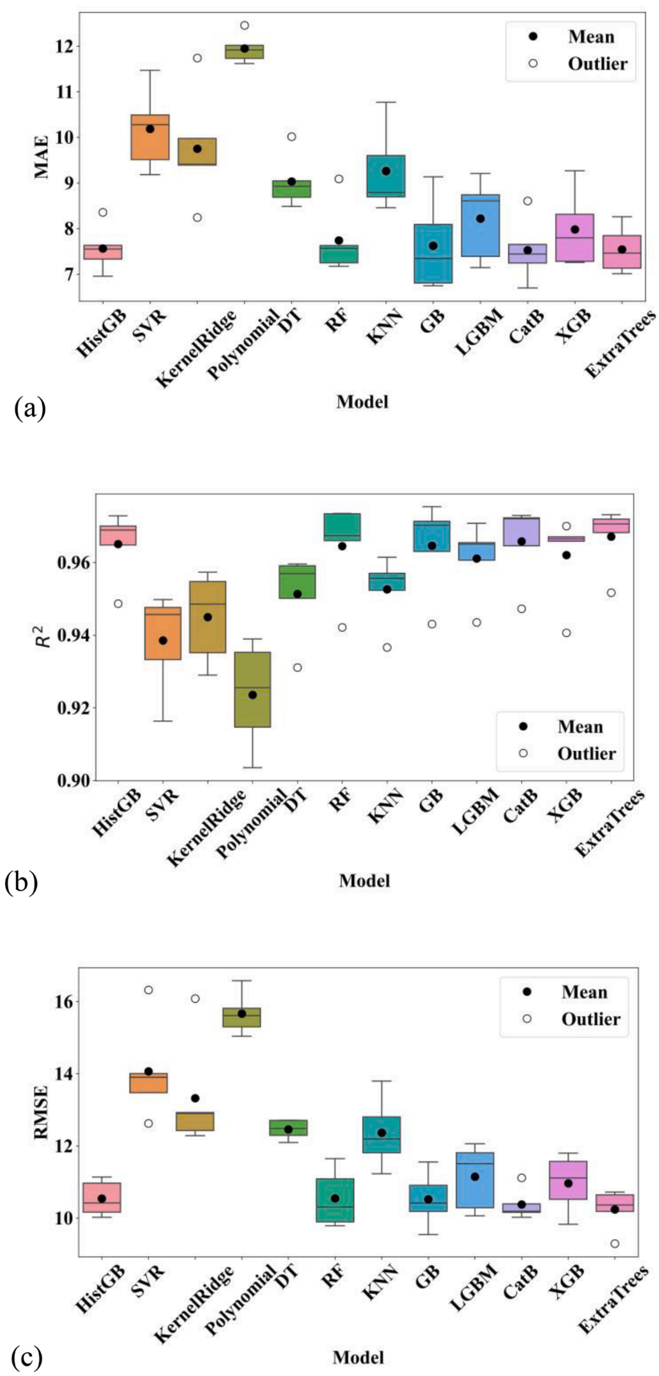

Fig. 10. Cross validation scores.

and MAE of (93.931 and 7.929) on training and testing sets, respectively. GB, XGBoost and LGBM also have high R^2 values around 0.960 on testing set and achieving relatively good RMSE and MAE values. These models employ boosting techniques that help to improve the prediction by trying to correct the mistakes made by the previous models. KNN performs fairly well with an R^2 of (0.990 and 0.945) on training and testing sets, respectively. However, its error rates are higher, with RMSE values of (5.703 and 13.372), and MAE values of (1.678 and 10.098) on training and testing sets, respectively, showing an inconsistency in performance. DT and KRR have relatively lower but still reasonable performance with R^2 values of 0.991 and 0.964 on training and 0.944 and 0.941 on testing datasets, respectively. DT has higher error rates with RMSE (5.616 and 13.533) and MAE (1.811 and 9.028) on training and testing sets, respectively which indicates that it might overfit the training data. KRR has RMSE values of (11.047 and 13.892), and MAE values of (7.931 and 10.207) on training and testing sets, respectively which shows it struggles with error minimization. SVR and PR have the lowest accuracy. SVR gives R^2 values of 0.960 on training and 0.947 on testing, with higher RMSE (11.603 on training and 13.080 on testing) and MAE (7.283 on training and 9.461 on testing). PR shows the lowest R^2 values (0.944 on training and 0.900 on testing) and the highest RMSE (13.698 on training and 18.010 on testing) and MAE (10.270 on training and 13.295 on testing), which means significant prediction errors and low model performance

The information provided in Table 3 is clearly depicted in the graphical representation shown in Fig. 12. This visualization allows for a more comprehensive comprehension of the performance metrics across various machine-learning models presented in Table 3.

6.3. Residual analysis of machine learning models

The residual plots for the entire dataset of all the ML models discussed in this study are presented in Fig. 13. From Fig. 13 it can be observed that there are significant variations in the predictive capacities of the models. The ETR model has the least mean residual (0.06 kN) and standard deviation of residuals (6.46 kN), hence, the predictions of this model are accurate and close to the actual values. Likewise, the HistGB model has a relatively small mean residual of 0.10 kN and a standard deviation of 6.61 kN, indicating a small amount of error spread and good predictive capability. On the other hand, the PR and SVR models have more dispersion with the mean of residuals of 0.47 kN and 0.43 kN; and the corresponding standard deviations of 14.66 kN and 11.91 kN, respectively. This implies that there is a higher variability in the prediction errors and this could be an indication of issues with the robustness and generalization of the model. The DT and KNN models also give reasonable results with the mean residuals of 0.07 kN and 0.13 kN, and standard deviations of 7.87 kN each. These results suggest fairly good performance of the model with a reasonable level of variability in the errors. However, it is observed that both the GB and LGBM models are slightly overestimated with positive mean residuals of 0.51 kN and 0.49 kN, respectively, and standard deviations around 8 kN. This overestimation trend could be attributed to the models' boosting mechanisms which while increasing the predictive power, might lead to slight bias under certain conditions. In general, the ETR and HistGB models have the lowest residuals, which proves their ability to minimize prediction errors. The differences of the residual characteristics among the models demonstrates how different learning algorithms and hyperparameters affect the model's performance. The ETR model's ensemble method helps to reduce the variance and hence the residuals are low while the boosting techniques in GB and LGBM, despite their sophistication, can lead to overfitting or inadequate regularization, and hence a slight overestimation.

6.4. Feature importance analysis

From the SHAP summary plot in Fig. 14, it is possible to provide a clear illustration of the relative importance of various features in predicting the shear strength (V_{pz}) of stainless-steel panel zones. The bolt diameter (D_b) is identified as the most influential factor accounting for about 28 % of the model's predictive power, with a mean SHAP value of about 17.5. Following D_b, the column second moment of inertia (I_{xx}^c) contributes 24 %, which underlines the significance of the column's section geometric properties in resisting shear forces. The bolt spacing between comparison bolts (P_c), contributing 18 %, reveals that having two bolt rows in the compression side is structurally beneficial as it increases the number of bolts and the overall resistance. Other features such as beam second moment of inertia (I_{xx}^b) and end-plate thickness (t_{ep}) also show considerable importance, each contributing around 10 %, which indicates their contribution to the enhancement of the

Table 3
performance of predictive models for V_{PZ} output.

Model	R^2			RMSE [kN]			MAE [kN]		
	Train	Test	All data	Train	Test	All data	Train	Test	All data
KRR	0.964	0.941	0.959	11.047	13.892	11.674	7.931	10.207	8.389
PR	0.944	0.900	0.935	13.698	18.010	14.667	10.270	13.295	10.877
DT	0.991	0.944	0.981	5.616	13.533	7.875	1.811	9.028	3.262
RF	0.990	0.964	0.985	5.793	10.777	7.082	3.931	7.929	4.735
ETR	0.992	0.968	0.987	5.057	10.306	6.464	2.664	7.196	3.575
KNN	0.990	0.945	0.981	5.703	13.372	7.869	1.678	10.098	3.370
GB	0.986	0.960	0.981	6.913	11.436	8.030	4.627	7.804	5.266
XGB	0.989	0.965	0.984	6.252	10.594	7.334	4.388	7.895	5.093
LGBM	0.986	0.950	0.979	6.940	12.709	8.423	4.511	9.020	5.417
CatBoost	0.992	0.968	0.987	5.314	10.217	6.599	3.426	7.562	4.257
HistGB	0.992	0.964	0.987	5.072	10.842	6.647	3.035	7.741	3.981
SVR	0.960	0.947	0.958	11.603	13.080	11.914	7.283	9.461	7.721

structural stability and resistance. The other less influential parameters such as the horizontal and vertical distances between bolts (g_i, P_i), the end plate width (b_{ep}) and the bolt spacing in tension (P_t) account for about 20 %.

6.5. Global explanation

The SHAP violin summary plot is employed to not only present the distribution of SHAP values but also to display the corresponding trends of influence on the model's outcomes. The SHAP violin summary plot for the predictive model of shear strength (V_{pz}) is illustrated in Fig. 15. The x-axis represents the SHAP value, which shows the impact on the model's output, while the y-axis lists the input features sorted by their importance. Each data point in the plot is color-coded from blue to red, which indicates the growth of feature values. The width of each violin represents the density of the SHAP values at different levels of impact. For example, higher values of bolt diameter (D_b), depicted in red towards the right, significantly increase the model's prediction of shear capacity, in accordance with the structural engineering understanding that larger bolts provide greater load-carrying capacity. Similarly, higher values of column second moment of inertia (I^c_{xx}), also shown in red on the right side, indicate a strong positive impact on shear capacity, which reflects the importance of column section properties in resisting shear forces. The feature bolt spacing between comparison bolts (P_c) has the same pattern where increased spacing (the right side highlighted with red color) positively affects shear capacity by optimizing bolt distribution and resistance. Some of the features that have moderate effect include the beam second moment of inertia (I^b_{xx}) and end-plate thickness (t_{ep}), where an increase in the value (red points) improves the shear capacity. On the other hand, features like horizontal distance between bolts (g_i), vertical distance (P_i), end-plate width (b_{ep}), and bolt spacing in tension (P_t) have relatively less effect as their SHAP values are close to zero meaning they have a less effect as compared to the major features. Notably, higher SHAP values of horizontal distance (g_i) lead to the negative effect on the shear capacity, which implies that larger horizontal distances between bolts may reduce structural effectiveness. This SHAP violin summary plot helps to understand the relative significance and the direction of the impact of each input parameter on the shear strength of stainless-steel panel zones and underlines the importance of geometric characteristics in determining structural performance and validating findings from existing structural engineering literature.

6.6. Local explanation

Individual explanation focuses on understanding the factors that affect the outcomes at the individual sample level. One approach to achieving this is through techniques like SHAP that provide a breakdown of the contributions of individual features to the output. These values represent the extent to which each feature influences the model's output. For ETR model (the best performing model in predicting shear strength), SHAP can be used to explain the prediction for specific samples and the contribution of each input variable. This approach decomposes the prediction into component contributions and sums up these to form the final prediction. The baseline prediction value is an average determined from the training dataset and is used as a reference point. Variation from this baseline is associated with the input features where visual indicators such as colored bars is employed to show positive or negative effects. This approach does not only quantifies the impact of each input on the predicted output but also brings out the fact that some outputs are more dependent on some feature inputs than on others, which emphasizes the non-uniform nature of input significance in individual predictions. Fig. 16(d) shows the explanation for a specific training dataset (sample 443) with a base value of 175.9 kN and an output value of 177.77 kN which is close to the FE value of 177.76 kN. From the example, it can be seen that the diameter of the bolt (D_b) and the second moment of area of the column (I^c_{xx}) have a significant influence on the predicted shear strength capacity. On the other hand, the distance between the compression bolts (P_c) is the most important characteristic that has a negative impact on the outcome.

7. GUI development

Based on the previous results, it can be concluded that the proposed method can effectively estimate the shear strength of stainless-steel column web panels. Therefore, the optimal ML model, namely ETR has been incorporated into a GUI application. A GUI that enables the users to operate the software through graphical elements like buttons and menus rather than text-based commands is a boost to accessibility.

This feature is quite useful for individuals who do not have a strong background in programming and allows them to employ the ML model for predicting the shear strength of column web panels in a way that minimizes input errors and allows users to explore multiple configurations efficiently. The GUI was implemented using Tkinter, one of the Python based libraries which is quite popular and easy to use. Tkinter is a standard Python interface to the Tcl/Tk GUI toolkit that is integral to Python and usually included with its installations. This library supports the creation of interactive interfaces by linking the user interface with the main software program through Object-Oriented Programming (OOP) principles.

This structure ensures a responsive and compatible user experience across various Python environments, making the interface easily deployable and adaptable.

Fig. 17 shows the GUI application through which the performance of the column web panels can be analyzed. The system allows the users to input the parameters in the "Feature Inputs" sub-section and the system calculates and presents the shear strength in the "Model Output" menu. All necessary resources including installation instructions, documentation, and source code for using or further customizing the GUI, are

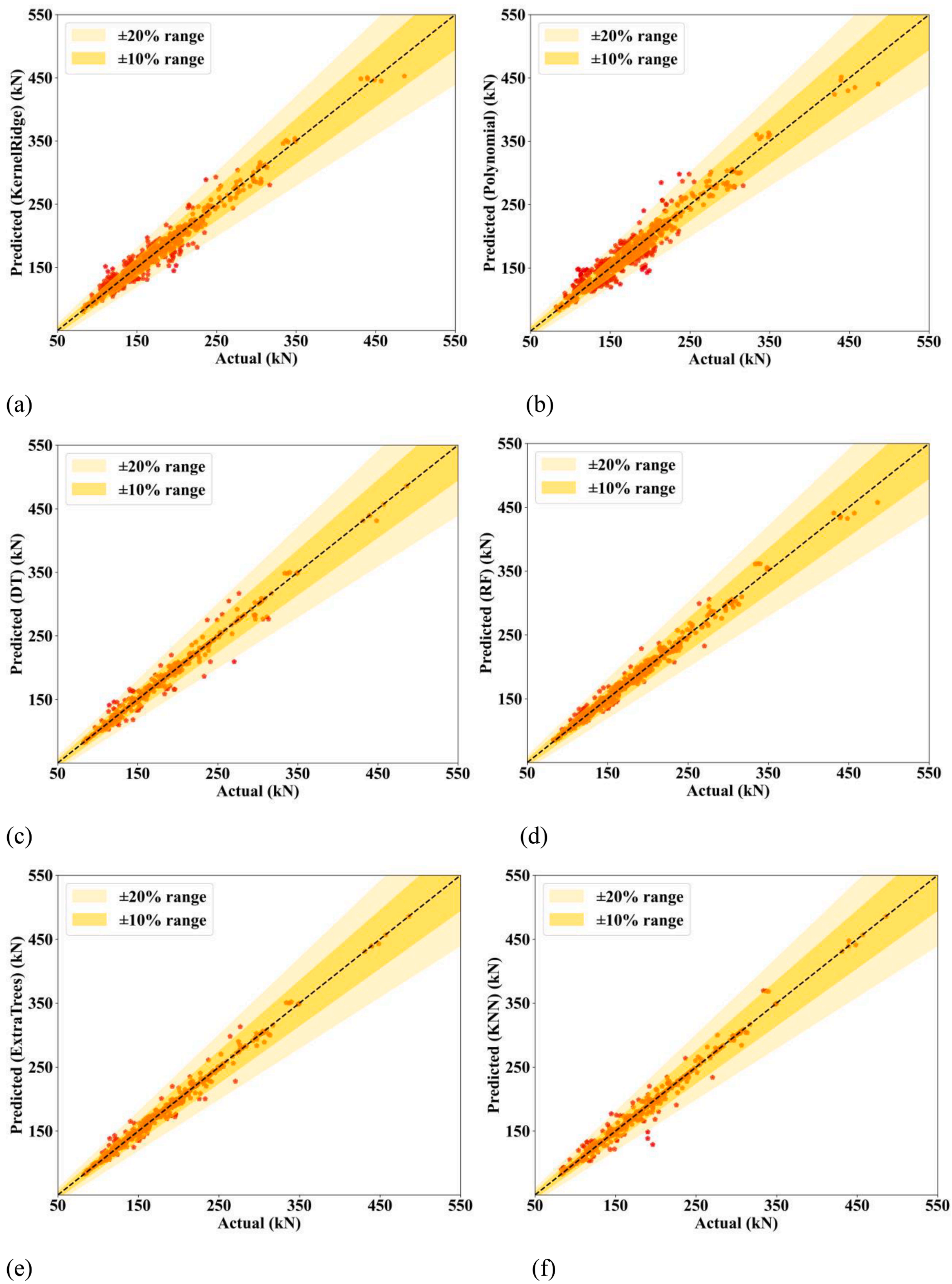

Fig. 11. Comparing the shear strength of panel zones between the predicted outcomes of machine learning models and the actual results.

available at the repository [68]. This makes the interface not only a practical tool for immediate use but also an adaptable resource for future research applications. Thus, the presented study provides a useful and efficient tool for engineers and researchers, as it combines the advanced machine learning models with the convenient GUI, which increases the applicability and generalization of the research outcomes.

By bridging sophisticated ML techniques with a straightforward interface, this GUI makes the research outcomes more accessible and

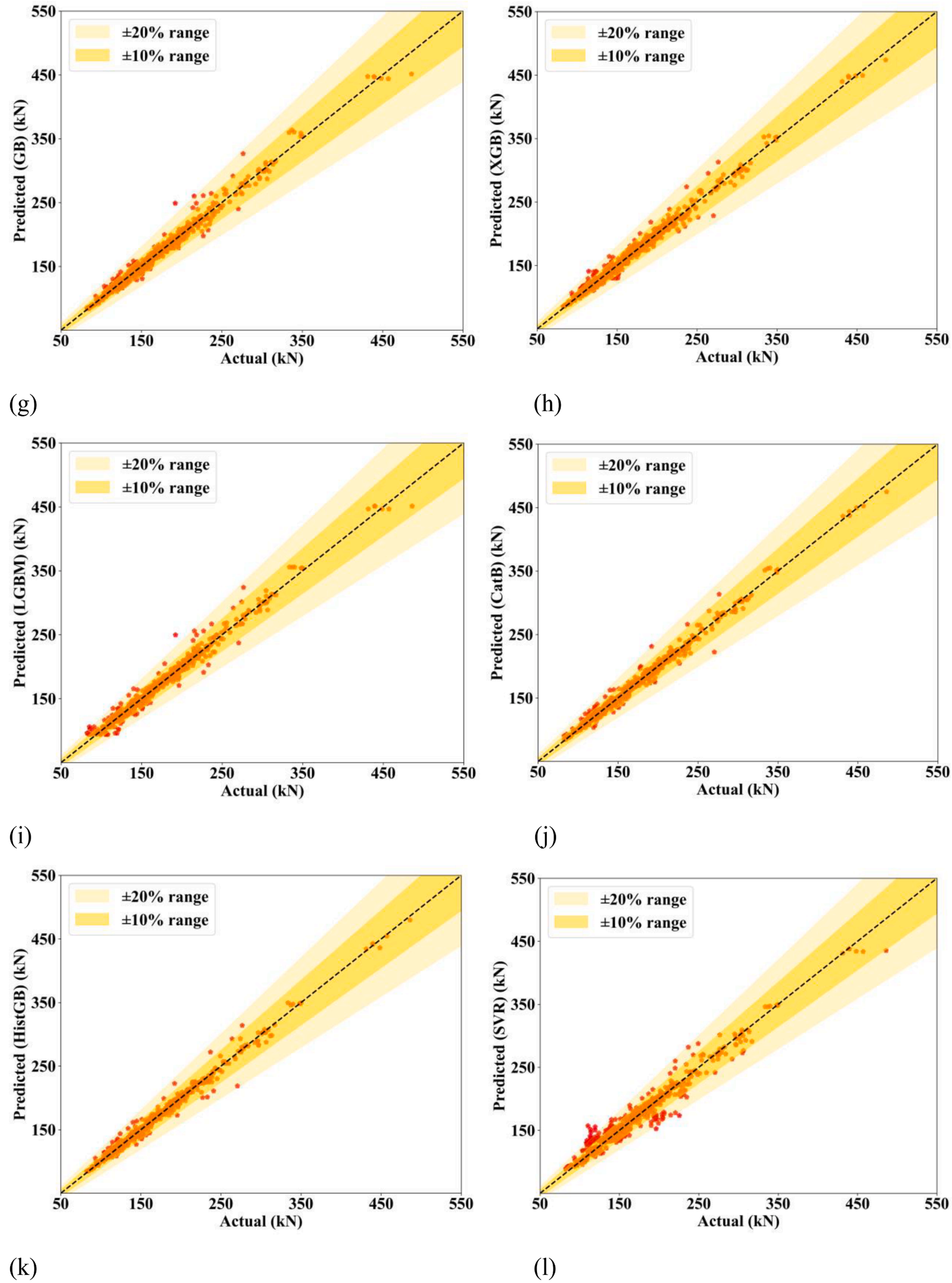

Fig. 11. (*continued*).

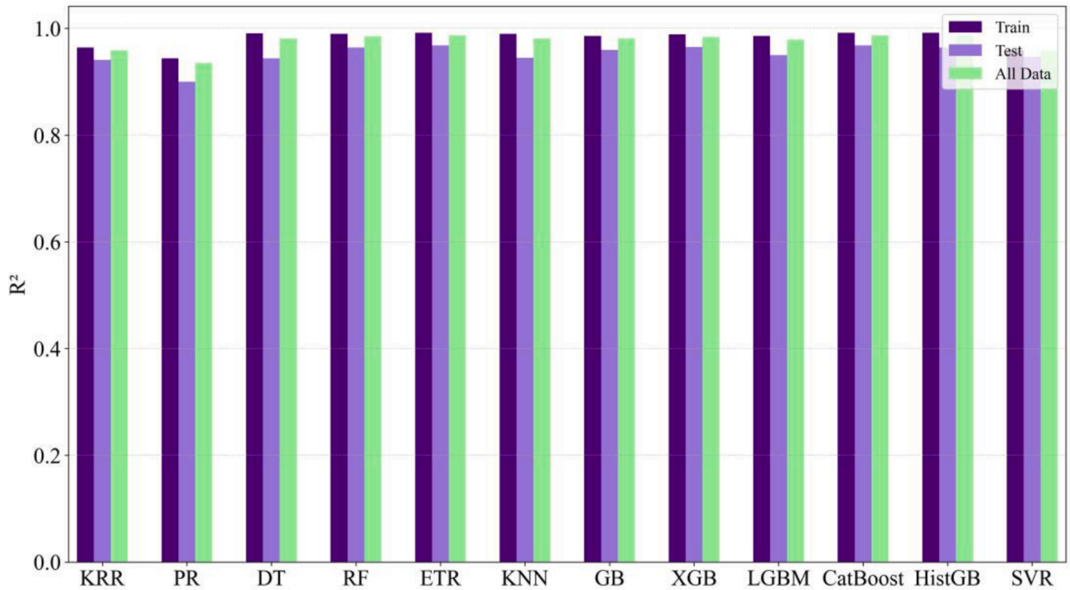

(a)

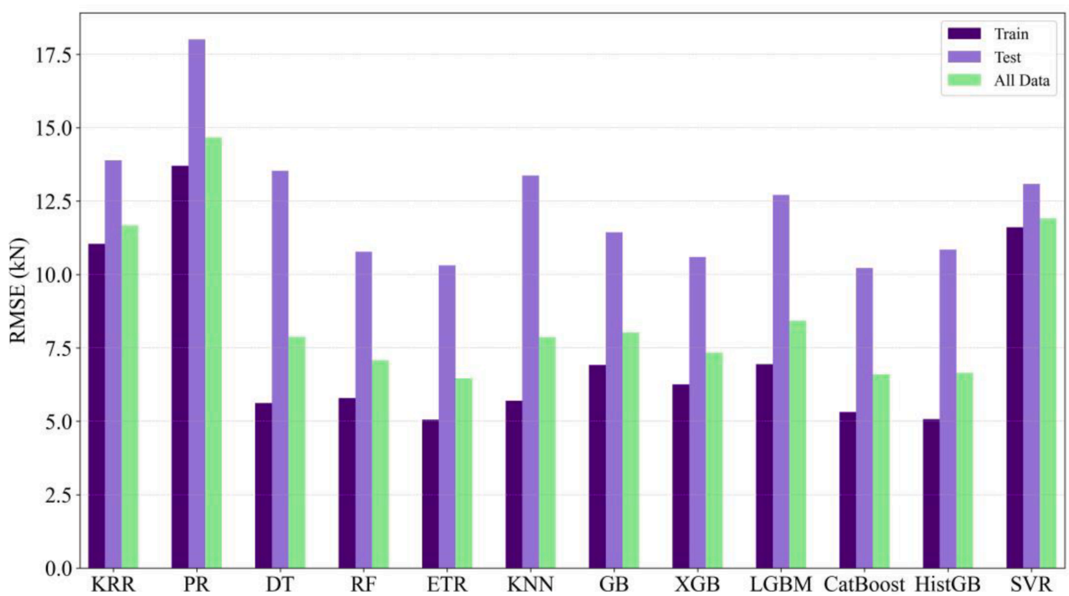

(b)

Fig. 12. Assessment of the performance of machine learning models.

actionable, contributing to broader applications and ease of integration in professional contexts.

8. Limitations and future research

This study's ML approach provides significant predictive accuracy but has several limitations. The dataset, although comprehensive, was constrained by the material grades and properties provided by the suppliers of stainless-steel sections, as recommended by the British Steel Association. As a result, these findings may not fully generalize to connections using materials with considerably different properties from those explored here. Given the distinct mechanical properties of various types of stainless steel, this study focused on the austenitic type due to its prevalent use in structural applications and the comprehensive material modeling recommendations available in Eurocode 3 Part 1–4 (EN 1993–1–4) [13].

Furthermore, this methodology was developed based on monotonic loading conditions only. Cyclic loading conditions, which are known to affect joint behavior, were not included in this research. Future studies could explore cyclic loading to determine if and how it influences the performance of stainless-steel column web panels. This predictive framework may require adaptation or further validation before generalizing to other loading conditions, material types, or joint configurations.

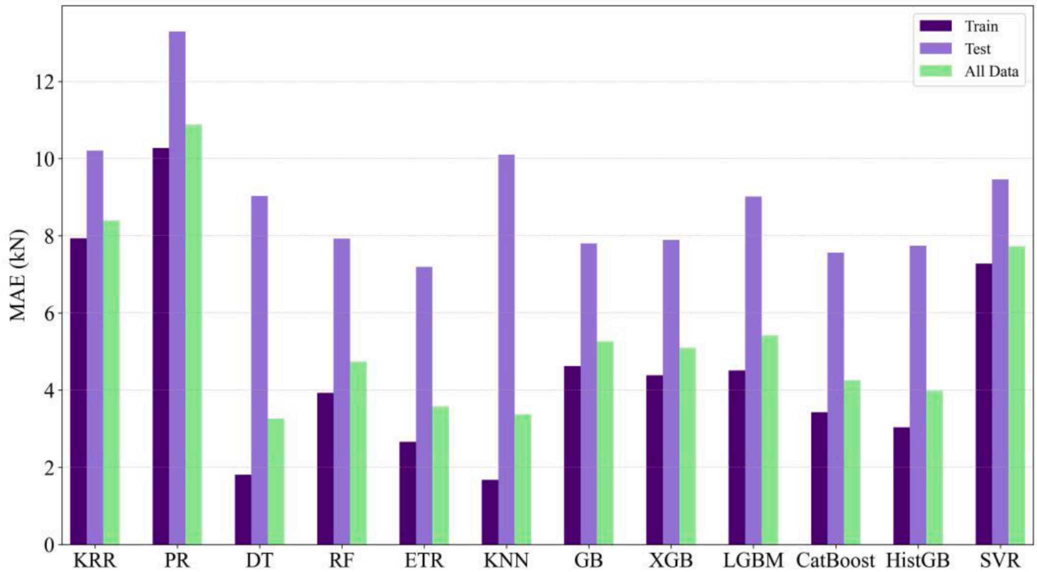

(c)

Fig. 12. (*continued*).

Future research should therefore focus on expanding the database of stainless-steel panel zone behaviors across a range of configurations and material types. This would enhance understanding of these elements and support the development of improved design practices. While this study was limited to standard H and I-shaped steel cross-sections, future work could incorporate other cross-section types, such as rectangular or circular hollow sections. It is acknowledged that other types, such as ferritic and duplex stainless steels, exhibit different mechanical characteristics. Future research could explore these types of stainless steel. A key area for further investigation is the interaction of axial forces with bending moments in beams and columns, as this interplay also impacts panel zone behavior. Another important direction for future research is using data-driven ML models to make stainless steel components more efficient. By focusing on optimization, future studies could help reduce material weight and costs, leading to structures that are both strong and more affordable. These improvements would make stainless steel more useful in different structural applications by creating lighter, yet durable, designs that meet performance needs while staying within budget.

The integration of this GUI tool into existing engineering practices presents potential advantages and limitations. By providing rapid, data-driven predictions, this GUI tool offers an efficient alternative to traditional methods, potentially streamlining workflows in preliminary design stages. However, broader validation of the tool in different structural contexts and configurations is necessary to ensure accuracy across diverse applications.

9. Conclusions

Machine learning (ML) provides engineers with substantial benefits by simplifying application process. Engineers can apply ML models using this approach, without having to understand the detailed physical aspects of the models, thus making possible integration of ML into many projects. Although training these models is time-consuming in terms of computational resources, the models can predict quickly which may be faster than traditional methods. For effective use of ML models in engineering, these models must be developed with a focus on transparency and clarity. This makes it possible for technical and non-technical individuals to comprehend the steps that were undertaken to arrive at predictions, which is important for instilling trust in the model's dependability. This study aims to develop an explainable machine-learning framework that can be used to predict the shear strength of stainless-steel column web panels. Subsequently, the most effective algorithms were identified and subjected to an explainable analysis utilizing the SHAP algorithm. The findings of this study are summarized as follows:

- The ETR and CatBoost have been determined to be the most optimal for all of the metrics and datasets employed.
- The R^2 value for ETR is the highest, with a training set value of 0.992 and a testing set value of 0.968. This indicates that the model fits the data well and possesses excellent predictive ability. Additionally, it consistently achieves the lowest RMSE values of (5.057 and 10.306) on the training and the testing sets, respectively, as well as the lowest MAE values of (2.664 and 7.196) on the training and the testing sets, respectively. This indicates that it has the fewest prediction errors.
- The SHAP results provide a thorough comprehension of the impacts that features have on the shear strength of column web panels. According to the SHAP results, the bolt diameter and the column's second moment of inertia are the two most influential input features that impact the shear strength.
- Based on the analysis of local explanations, the model's predictions tend to rely more on individual features rather than complex interactions among all variables.
- The final phase of this research involves the creation of a graphical user interface GUI application, which employs the best machine learning model performer (ETR) to estimate the shear strength of column web panels.
- This study's findings hold practical implications for structural design and engineering. The showed accuracy and transparency of the machine learning model, particularly with integrating SHAP for interpretability, suggests that such approaches could serve as important tools in structural assessments.
- By providing reliable and accessible predictions of shear strength for stainless-steel column web panels, this method has the potential to supplement traditional design methods, offering a data-driven, efficient alternative for complex structural components.

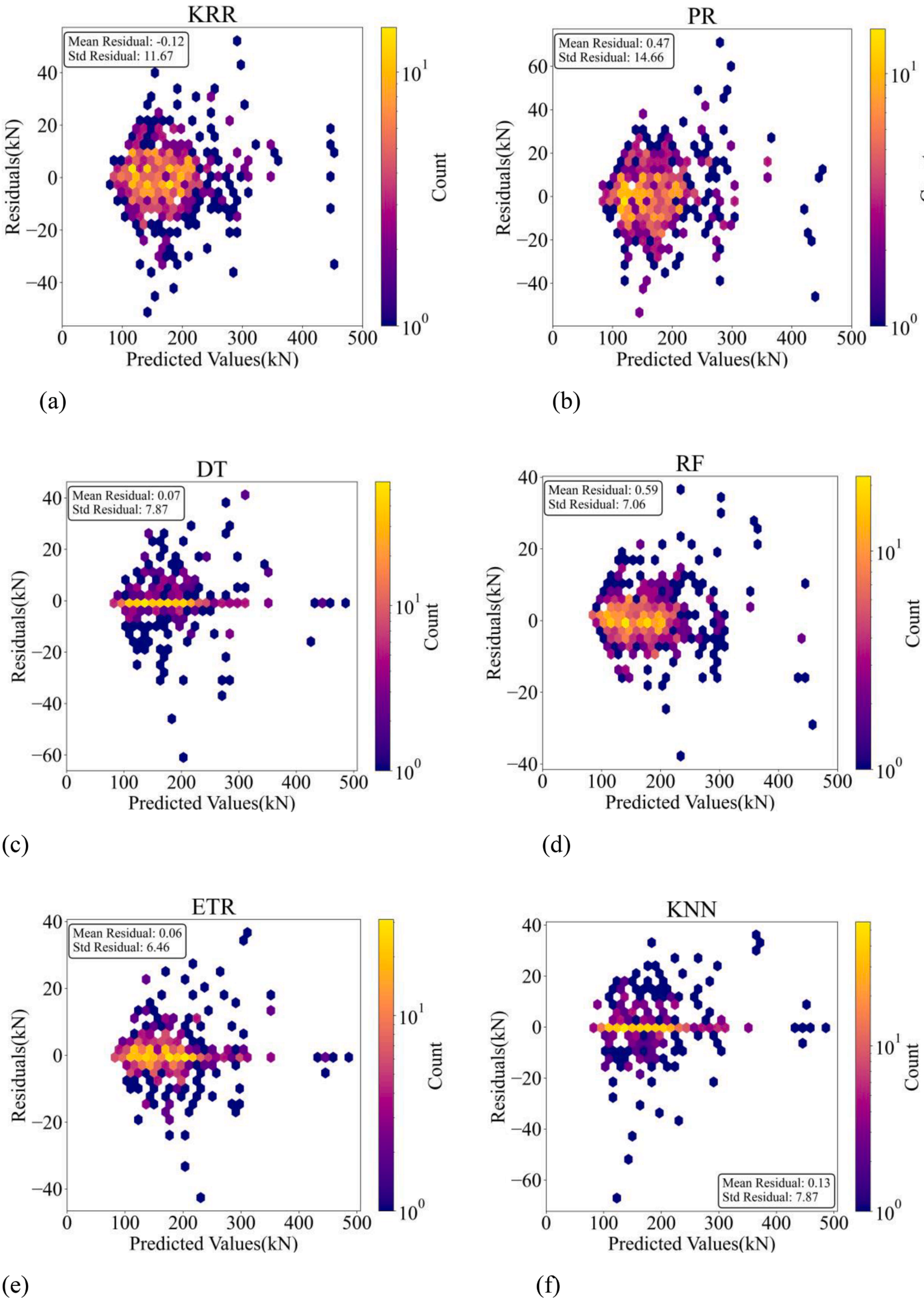

Fig. 13. Comparing the residuals of shear strength predictions across various machine learning algorithms.

- Additionally, insights from this model could inform potential updates to design guidelines, ensuring that they better reflect the unique mechanical behavior of stainless steel.

Such advancements could facilitate wider adoption of stainless-steel in structural design, while promoting the use of machine learning tools in engineering practice.

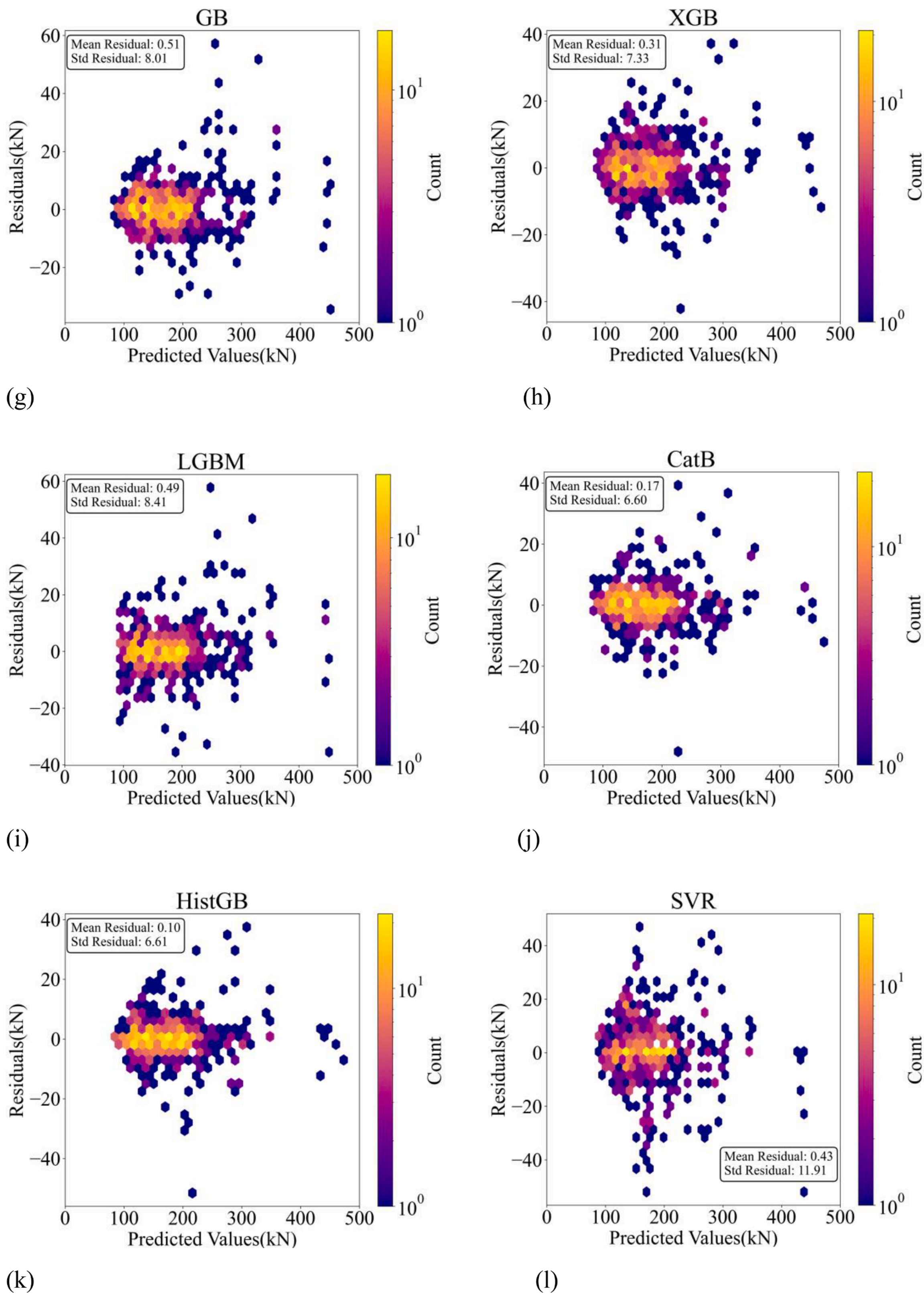

Fig. 13. (*continued*).

CRediT authorship contribution statement

Sina Sarfarazi: Writing – original draft, Validation, Data curation, Software. **Rabee Shamass:** Supervision, Methodology. **Federico Guarracino:** Writing – review & editing, Visualization, Supervision, Methodology. **Ida Mascolo:** Writing – review & editing, Methodology. **Mariano Modano:** Supervision.

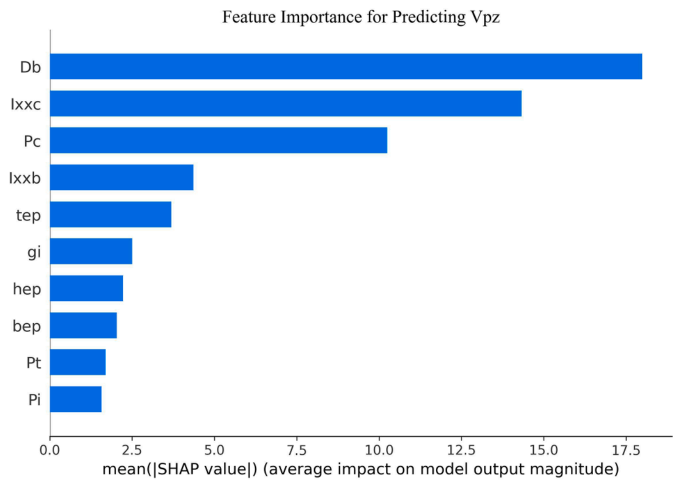

Fig. 14. Feature importance plot.

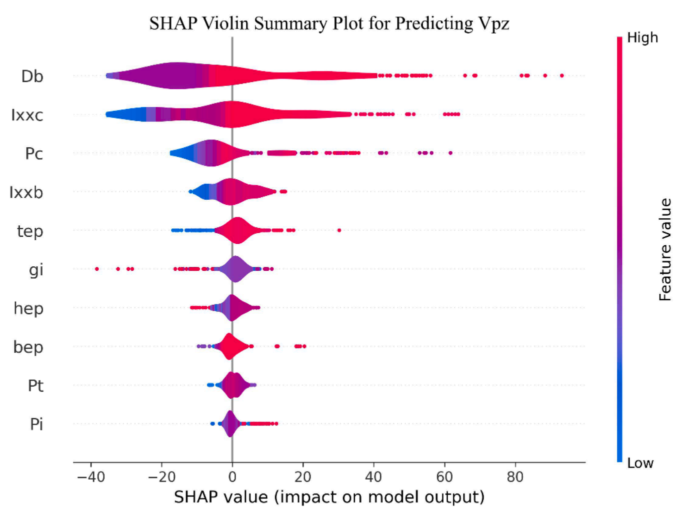

Fig. 15. SHAP violin summary plot.

Declaration of competing interest

The authors declare that they have no known competing financial interests or personal relationships that could have appeared to influence the work reported in this paper.

Appendix A

Table of Annotations

Term	Description
Adaptive Neuro-Fuzzy Inference System	ANFIS
Artificial Neural Networks	ANN
artificial intelligence	AI
beam second moment of inertia	I_{xx}^{b}
bolt diameter	D_b
bolt spacing between comparison bolts	P_c
bolt spacing in tension	P_t
Categorical Boosting	CatBoost
Coefficient of Determination	R^2
Column second moment of inertia	I_{xx}^{c}
Decision Tree	DT
End-plate height	h_{ep}
End-plate thickness	t_{ep}

(*continued on next page*)

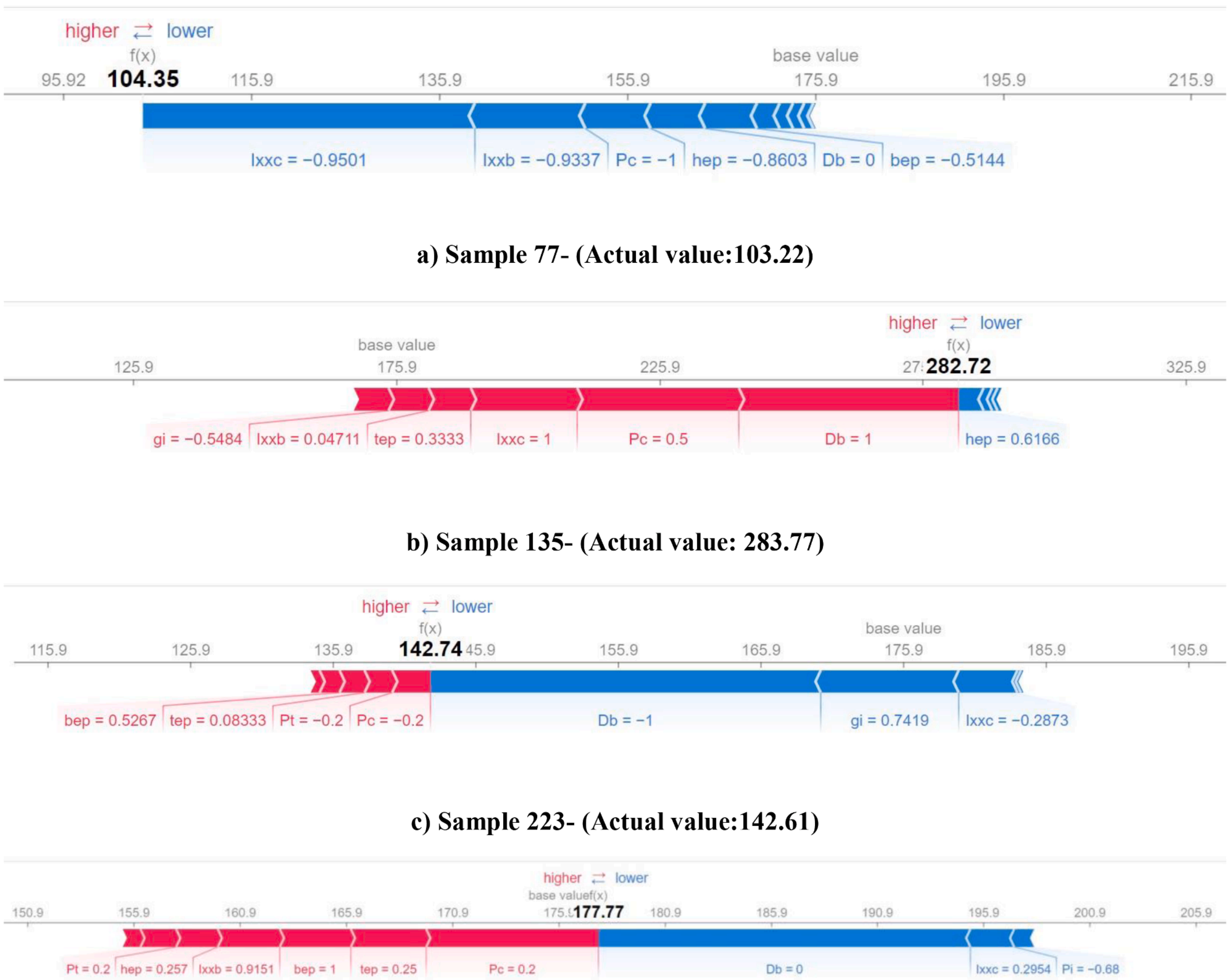

a) Sample 77- (Actual value:103.22)

b) Sample 135- (Actual value: 283.77)

c) Sample 223- (Actual value:142.61)

d) Sample 443- (Actual value:177.76)

Fig. 16. SHAP individual force plots for selected samples.

(*continued*)

Term	Description
End-plate width	b_{ep}
Exclusive Feature Bundling	EFB
Explainable artificial intelligence	XAI
Extreme Learning Machine	ELM
Extreme Gradient Boosting	XGBoost
Extremely Randomized Trees	ETR
Finite element	FE
Flush end-plate connections	FECs
Gradient Boosting	GB
Gradient Boosting Decision Trees	GBDT
Gradient-based One-Side Sampling	GOSS
Graphical user interface	GUI
Genetic Programming	GP
Histogram-Based Gradient Boosting	HistGB
Horizontal distance between bolts	g_i
Interquartile range	IQR
K-Nearest Neighbors	KNN
Kernel Ridge Regression	KRR
Light Gradient Boosting	LGBM
Linear Genetic Programming	LGP
Machine learning	ML
Mean absolute percentage error	MAPE
Mean Absolute Error	MAE
Moment-resisting frame	MRF

(*continued on next page*)

Fig. 17. The developed GUI.

(*continued*)

Term	Description
Multi-Linear Regression	MLR
Object-Oriented Programming	OOP
Panel zone	PZ
Polynomial Regression	PR
Radial basis function	RBF
Random Forest	RF
Reinforced concrete	RC
Root Mean Square Error	RMSE
SHapley Additive exPlanations	SHAP
Shear strength of the panel zone	V_{pz}
Support Vector Regression	SVR
Support vector machines	SVM
vertical distance between the innermost tension bolt and the innermost comparison bolt	P_i

Data availability

Data will be made available on request.

References

[1] M. Rabi, R. Shamass, K.A. Cashell, Experimental investigation on the flexural behaviour of stainless-steel reinforced concrete beams, Struct. Infrastruct. Eng. (2022), https://doi.org/10.1080/15732479.2022.2065687.
[2] L. Gardner, The use of stainless-steel in structures, Prog. Struct. Mater. Eng. 7 (2) (2005) 45–55, https://doi.org/10.1002/pse.190.
[3] H. Rahimpour, A.B. Amini, F. Sharifi, A. Fahmi, S. Zinatloo-Ajabshir, Facile fabrication of next-generation sustainable brick and mortar through geopolymerization of construction debris, Sci. Rep. 14 (1) (2024) 10914, https://doi.org/10.1038/s41598-024-61688-x.
[4] C. Wang, J. Guo, L. Cao, Y. Zhang, C. Li, Z. Ma, Mechanical behavior and fiber reinforcing mechanism of high-toughness recycled aggregate concrete under high strain-rate impact loads, Constr. Build. Mater. 437 (2024) 136960, https://doi.org/10.1016/j.conbuildmat.2024.136960.
[5] C. Wang, J. Yuan, B. Lu, Y. Zhang, Z. Ma, New insights into the mechanical behavior and enhancement mechanism of micro-steel-fiber-reinforced recycled aggregate concrete through in-situ 4D CT analysis, Constr. Build. Mater. 438 (2024) 137111, https://doi.org/10.1016/j.conbuildmat.2024.137111.
[6] C. Wang, Z. Du, Microscopic interface deterioration mechanism and damage behavior of high-toughness recycled aggregate concrete based on 4D in-situ CT experiments, Cem. Concr. Compos. 153 (2024) 105720, https://doi.org/10.1016/j.cemconcomp.2024.105720.
[7] R. Shamass, F. Guarracino, Numerical and theoretical modeling of the web-post buckling of stainless-steel cellular beams, in: *ce/papers, 4,* EUROSTEEL 2021 Sheffield-Steel's coming home, 2021, pp. 1551–1557, https://doi.org/10.1002/cepa.1455.
[8] L. Gardner, Stability and design of stainless steel structures – review and outlook, Thin Walled Struct. 141 (2019) 208–216.
[9] I. Mascolo, F. Guarracino, S. Sarfarazi, G. Della Corte, A proposal for a simple characterization of stainless steel connections through an equivalent yield strength, Structures 68 (2024) 107043, https://doi.org/10.1016/j.istruc.2024.107043.
[10] S. Sarfarazi, R. Shamass, I. Mascolo, G. Della Corte, F. Guarracino, Some considerations on the behaviour of bolted stainless-steel beam-to-column connections: a simplified analytical approach, Metals (Basel) 13 (2023) 753, https://doi.org/10.3390/met13040753.
[11] Z. Chen, J. Yao, B. Zheng, G. Shu, Classification and ultimate capacity of duplex stainless steel H-section under cyclic loading, J. Constr. Steel Res. 218 (2024) 108725, https://doi.org/10.1016/j.jcsr.2024.108725.
[12] Comité Européen de Normalisation [CEN], Eurocode 3: Design of Steel Structures – Part 1-8: Design of Joints (EN 1993-1-8), CEN, Brussels, Belgium, 2005.

[13] European Committee for Standardization (CEN), *Eurocode 3: Design of Steel Structures – Part 1-4: General Rules – Supplementary Rules For Stainless Steels.* EN 1993-1-4:2006, CEN, Brussels, Belgium, 2006.
[14] S. Sarfarazi, A. Fakhraddini, K. Modaresahmadi, Evaluation of panel zone shear strength in cruciform columns, box-columns and double-web columns, Int. J. Struct. Civil Eng. Res. 5 (1) (2016) 52–56, https://doi.org/10.18178/ijscer.5.1.52-56.
[15] R. Zandonini, O.S. Bursi, Monotonic and hysteretic behavior of bolted endplate beam-to-column joints, J. Adv. Steel Struct. 1 (2002) 81–94.
[16] H. Saffari, S. Sarfarazi, A. Fakhreddini, A mathematical steel panel zone model for flanged cruciform columns, Steel and Composite Structures 20 (4) (2016) 851–867.
[17] S. Sarfarazi, H. Saffari, A. Fakhraddini, Shear behavior of panel zone considering axial force for flanged cruciform columns, Civil Engineering Infrastructures Journal 53 (2) (2020) 359–377.
[18] H. Krawinkler, V.V. Bertero, E.P. Popov, *Inelastic Behavior of Steel Beam-To-Column Sub Assemblages* (EERC Rep. No. 71-7), University of California, Berkeley, CA, USA, 1971.
[19] J. Jin, S. El-Tawil, Evaluation of FEMA-350 seismic provisions for steel panel zones, Journal of Structural Engineering, ASCE 131 (2) (2005) 250–258.
[20] M.M. Shamszadeh, S. Maleki, Evaluation of strong column-weak beam criterion in spliced columns of steel moment frames, Results in Engineering 14 (2022) 100453, https://doi.org/10.1016/j.rineng.2022.100453.
[21] J.-P. Jaspart, *Recent Advances in the Field of Steel joints; Column Bases and Further Configurations For Beam-To-Column Joints and Beam Splices* (Professorship Thesis), University of Liège, Liège, Belgium, 1997, https://doi.org/10.48518/2268/30425.
[22] A.M. Girão Coelho, F.S.K. Bijlaard, H. Kolstein, Experimental behaviour of high strength steel web shear panels, Eng. Struct. 31 (7) (2009) 1543–1555, https://doi.org/10.1016/j.engstruct.2009.02.023.
[23] S. Jordão, L. Simões Da Silva, R. Simões, Behaviour of welded beam-to-column joints with beams of unequal depth, J. Constr. Steel Res. 91 (2013) 42–59, https://doi.org/10.1016/j.jcsr.2013.07.023.
[24] M. Tuna, C. Topkaya, Panel zone deformation demands in steel moment resisting frames, J. Constr. Steel Res. 110 (2015) 65–75, https://doi.org/10.1016/j.jcsr.2015.02.017.
[25] G. Brandonisio, A. De Luca, E. Mele, Shear strength of panel zone in beam-to-column connections, J. Constr. Steel Res. 71 (2012) 129–142, https://doi.org/10.1016/j.jcsr.2011.11.004.
[26] S. Lu, M. Wang, X. Han, T. Yin, Seismic performance analysis of semi-rigid steel frame based on panel zone mechanical characteristics of the joint experiment study, KSCE J. Civ. Eng. 28 (5) (2024) 1960–1979, https://doi.org/10.1007/s12205-024-1482-9.
[27] H.-T. Thai, Machine learning for structural engineering: a state-of-the-art review, Structures 38 (2022) 448–491, https://doi.org/10.1016/j.istruc.2022.02.003.
[28] D. Meng, S. Yang, H. Yang, A.M.P. De Jesus, J. Correia, S.-P. Zhu, Intelligent-inspired framework for fatigue reliability evaluation of offshore wind turbine support structures under hybrid uncertainty, Ocean Eng. 307 (2024) 118213, https://doi.org/10.1016/j.oceaneng.2024.118213.
[29] S. Mangalathu, H. Jang, S.-H. Hwang, J.-S. Jeon, Data-driven machine-learning-based seismic failure mode identification of reinforced concrete shear walls, Eng. Struct. 208 (2020) 110331, https://doi.org/10.1016/j.engstruct.2020.110331.
[30] S. Yang, Z. He, J. Chai, D. Meng, W. Macek, R. Branco, S.-P. Zhu, A novel hybrid adaptive framework for support vector machine-based reliability analysis: a comparative study, Structures 58 (2023) 105665, https://doi.org/10.1016/j.istruc.2023.105665.
[31] S.N.R. Shah, N.H. Ramli Sulong, A. El-Shafie, New approach for developing soft computational prediction models for moment and rotation of boltless steel connections, Thin Walled Struct. 133 (2018) 206–215, https://doi.org/10.1016/j.tws.2018.09.032.
[32] Y. Cao, K. Wakil, R. Alyousef, K. Jermsittiparsert, L. Si Ho, H. Alabduljabbar, A. Alaskar, F. Alrshoudi, A. Mustafa Mohamed, Application of extreme learning machine in behavior of beam to column connections, Structures 25 (2020) 861–867, https://doi.org/10.1016/j.istruc.2020.03.058.
[33] Kueh, Artificial neural network and regressed beam-column connection explicit mathematical moment-rotation expressions, J. Build. Eng. 43 (2021) 103195, https://doi.org/10.1016/j.jobe.2021.103195.
[34] S. Alagundi, T. Palanisamy, Neural network prediction of joint shear strength of exterior beam-column joint, Structures 37 (2022) 1002–1018, https://doi.org/10.1016/j.istruc.2022.01.013.
[35] J.H. Haido, Prediction of the shear strength of RC beam-column joints using new ANN formulations, Structures 38 (2022) 1191–1209, https://doi.org/10.1016/j.istruc.2022.02.046.
[36] H.S. Marie, K.A. El-Hassan, E.M. Almetwally, M.A. El-Mandouh, Joint shear strength prediction of beam-column connections using machine learning via experimental results, Case Studies in Construction Materials 17 (2022) 1–17, https://doi.org/10.1016/j.cscm.2022.04.020.
[37] A.A.H. Alwanas, A.A. Al-Musawi, S.Q. Salih, H. Tao, M. Ali, Z.M. Yaseen, Load-carrying capacity and mode failure simulation of beam-column joint connection: application of self-tuning machine learning model, Eng. Struct. 194 (2019) 220–229.
[38] S.H. Park, D. Yoon, S. Kim, Z.W. Geem, Deep neural network applied to joint shear strength for exterior RC beam-column joints affected by cyclic loadings, Structures 33 (2021) 1819–1832.
[39] T. Liu, Z. Wang, J. Zeng, J. Wang, Machine-learning-based models to predict shear transfer strength of concrete joints, Eng. Struct. 249 (2021) 113253.
[40] S. Zakir Sarothi, K. Sakil Ahmed, N. Imtiaz Khan, A. Ahmed, M.L. Nehdi, Predicting bearing capacity of double shear bolted connections using machine learning, Eng. Struct. 251 (2022) 113497.
[41] H. Naderpour, M. Sharei, P. Fakharian, M.A. Heravi, Shear strength prediction of reinforced concrete shear wall using ANN, GMDH-NN and GEP, Journal of Soft Computing in Civil Engineering 6 (1) (2022) 66–87, https://doi.org/10.22115/SCCE.2022.283486.1308.
[42] S. Mangalathu, J.-S. Jeon, Classification of failure mode and prediction of shear strength for reinforced concrete beam-column joints using machine learning techniques, Eng. Struct. 160 (2018) 85–94.
[43] ABAQUS, Inc. (2022). *ABAQUS Analysis User's Manual (Version 6.12)*. Dassault Systèmes.
[44] F. Pedregosa, G. Varoquaux, A. Gramfort, V. Michel, B. Thirion, O. Grisel, É. Duchesnay, Scikit-learn: machine learning in Python, J. Mach. Learn Res. 12 (2011) 2825–2830.
[45] V. Vovk, Kernel ridge regression. Empirical Inference: Festschrift in Honor of Vladimir N. Vapnik, Springer Berlin Heidelberg, Berlin, Heidelberg, 2013, pp. 105–116.
[46] E. Ostertagová, Modelling using polynomial regression, Procedia Eng 48 (2012) 500–506.
[47] G.A. Seber, A.J. Lee, Polynomial regression. Linear Regression Analysis, 2003, pp. 165–185.
[48] A. Husnain, M. Iqbal, H.A. Waqas, M. El-Meligy, M.F. Javed, R. Ullah, Machine learning techniques for predicting the peak response of reinforced concrete beam subjected to impact loading, Results in Engineering 24 (2024) 103135, https://doi.org/10.1016/j.rineng.2024.103135.
[49] G. Hajdú, N. Bektaş, A. Müller, Machine learning models for the elastic-critical buckling moment of sinusoidal corrugated web beam, Results in Engineering 23 (2024) 102371, https://doi.org/10.1016/j.rineng.2024.102371.
[50] A. Jimenez Rios, M.E.A. Ben Seghier, V. Plevris, J. Dai, Explainable ensemble learning framework for estimating corrosion rate in suspension bridge main cables, Results in Engineering 23 (2024) 102723, https://doi.org/10.1016/j.rineng.2024.102723.
[51] L. Breiman, Random forests, Mach Learn 45 (2001) 5–32.
[52] P. Geurts, D. Ernst, L. Wehenkel, Extremely randomized trees, Mach Learn 63 (2006) 3–42.
[53] P. Thisovithan, H. Aththanayake, D.P.P. Meddage, I.U. Ekanayake, U. Rathnayake, A novel explainable AI-based approach to estimate the natural period of vibration of masonry infill reinforced concrete frame structures using different machine learning techniques, Results in Engineering 19 (2023) 101388, https://doi.org/10.1016/j.rineng.2023.101388.
[54] H.F. Isleem, N.D.K.R. Chukka, A. Bahrami, S. Oyebisi, R. Kumar, T. Qiong, Nonlinear finite element and analytical modelling of reinforced concrete filled steel tube columns under axial compression loading, Results in Engineering 19 (2023) 101341, https://doi.org/10.1016/j.rineng.2023.101341.
[55] T. Chen, C. Guestrin, XGBoost: a scalable tree boosting system, in: Proceedings of the 22nd ACM SIGKDD International Conference on Knowledge Discovery and Data Mining, 2016, pp. 785–794.
[56] G. Ke, Q. Meng, T. Finley, T. Wang, W. Chen, W. Ma, T.-Y. Liu, LightGBM: a highly efficient gradient boosting decision tree, in: Proceedings of the 31st International Conference on Neural Information Processing Systems, 2017, pp. 3149–3157.
[57] M. Rabi, Y.S. Jweihan, I. Abarkan, F.P.V. Ferreira, R. Shamass, V. Limbachiya, K. D. Tsavdaridis, L.F.P. Santos, Machine learning-driven web-post buckling resistance prediction for high-strength steel beams with elliptically-based web openings, Results in Engineering 21 (2024) 101749, https://doi.org/10.1016/j.rineng.2024.101749.
[58] X. Liu, L. Yang, Z. Wang, et al., UAV-assisted wind turbine counting with an image-level supervised deep learning approach, IEEE Journal on Miniaturization for Air and Space Systems 4 (1) (2022) 18–24.
[59] S.M. Lundberg, S.I. Lee, A unified approach to interpreting model predictions. Advances in Neural Information Processing Systems, 2017, p. 30.
[60] S. Sarfarazi, R. Shamass, G. Della Corte, F. Guarracino, Assessment of design approaches for stainless-steel joints through an equivalent FE modelling technique, ce/papers 5 (4) (2022) 271–281, https://doi.org/10.1002/cepa.1756.
[61] K.J. Rasmussen, Full range stress-strain curves for stainless-steel alloys, J. Constr. Steel Res. 59 (1) (2003) 47–61, https://doi.org/10.1016/S0143-974X(02)00018-4.
[62] M.M. Eladly, B.W. Schafer, Numerical and analytical study of stainless-steel beam-to-column extended end-plate connections, Eng. Struct. 240 (2021) 112392, https://doi.org/10.1016/j.engstruct.2021.112392.
[63] A. Breda, S. Coppietres, T. Kuwabara, D. Debruyyne, The effect of plastic anisotropy on the calibration of an equivalent model for clinched connections, Thin Walled Struct. 145 (2019) 106360, https://doi.org/10.1016/j.tws.2019.106360.
[64] J.D. Gao, H.X. Yuan, X.X. Du, X.B. Hu, M. Theofanous, Structural behaviour of stainless steel double extended end-plate beam-to-column joints under monotonic loading, Thin Walled Struct. 151 (2020) 106743, https://doi.org/10.1016/j.tws.2020.106743.
[65] M. Elflah, M. Theofanous, S. Dirar, H.X. Yuan, Behavior of stainless-steel beam to column joints – Part 1: experimental investigation, J. Constr. Steel Res. 152 (2019) 183–193, https://doi.org/10.1016/j.jcsr.2018.02.040.

[66] Y. Song, D. Li, B. Uy, J. Wang, Ultimate behaviour and rotation capacity of stainless-steel end-plate connections, Steel and Composite Structures 42 (4) (2022) 569–590, https://doi.org/10.12989/scs.2022.42.4.569.
[67] British Stainless-steel Association, BSSA Stainless-Steel Sections Directory, 2nd ed., 2006. Retrieved from, https://bssa.org.uk/bssa_articles/bssa-stainless-steel-sections-directory-all-parts/.
[68] Sarfarazi S. (2024). Predicting Shear Strength in Stainless Steel Column Web Panels GUI. https://github.com/Sinasrfz/Predicting-Shear-Strength-in-Stainless-Steel-Column-Web-Panels-GUI-.git.